DETECTION OF ELECTRO-EXPLOSIVE DETONATORS BY RF SIGNATURE

A THESIS SUBMITTED TO
THE GRADUATE SCHOOL OF NATURAL AND APPLIED SCIENCES
OF
MIDDLE EAST TECHNICAL UNIVERSITY

BY

ÖZGEHAN KILIÇ

IN PARTIAL FULFILLMENT OF THE REQUIREMENTS
FOR
THE DEGREE OF DOCTOR OF PHILOSOPHY
IN
ELECTRICAL AND ELECTRONICS ENGINEERING

APRIL 2019

Approval of the thesis:

DETECTION OF ELECTRO-EXPLOSIVE DETONATORS BY RF SIGNATURE

submitted by **ÖZGEHAN KILIÇ** in partial fulfillment of the requirements for the degree of **Doctor of Philosophy in Electrical and Electronics Engineering Department, Middle East Technical University** by,

Prof. Dr. Halil Kalıpçılar
Dean, Graduate School of **Natural and Applied Sciences**

Prof. Dr. Tolga Çiloğlu
Head of Department, **Electrical and Electronics Engineering**

Prof. Dr. Şimşek Demir
Supervisor, **Electrical and Electronics Engineering Dept., METU**

Examining Committee Members:

Prof. Dr. Sencer Koç
Electrical and Electronics Engineering Dept., METU

Prof. Dr. Şimşek Demir
Electrical and Electronics Engineering Dept., METU

Prof. Dr. Erdem Yazgan
Electrical and Electronics Engineering Dept., TED University

Prof. Dr. Gönül Turhan Sayan
Electrical and Electronics Engineering Dept., METU

Prof. Dr. Birsen Saka
Electrical and Electronics Engineering Dept., Hacettepe University

Date: 03.04.2019

I hereby declare that all information in this document has been obtained and presented in accordance with academic rules and ethical conduct. I also declare that, as required by these rules and conduct, I have fully cited and referenced all material and results that are not original to this work.

Name, Last name : Özgehan Kılıç

Signature :

ABSTRACT

DETECTION OF ELECTRO-EXPLOSIVE DETONATORS BY RF SIGNATURE

Kılıç, Özgehan
Ph.D., Department of Electrical and Electronics Engineering
Supervisor: Prof. Dr. Şimşek Demir

April 2019, 80 pages

Electro-Explosive Detonator (EED) is the main trigger mechanism in most of the explosive systems. Explosion of these systems start with the burning of the EED bridge wire by excess current, followed by the explosion of higher amount of explosives. Accidental or on purpose explosion of these explosives results in many losses. The electrical properties of the EEDs are modeled at the microwave frequencies, but there is no focus on the detection of EEDs by their RF signature. MUltiple SIgnal Classification (MUSIC) and Prony's methods are adopted for this purpose, and measurements are conducted for justifying the methods. A Multiple Input Multiple Output (MIMO) measurement system is also setup and detection performance enhancement is achieved by statistical MIMO application.

Keywords: Detection, RF Signature, MUSIC Method, Prony's Method, MIMO

ÖZ

ELEKTRO-PATLAYICI DETONATÖRLERİN RF İMZA İLE TESPİTİ

Kılıç, Özgehan
Doktora, Elektrik ve Elektronik Mühendisliği
Tez Yöneticisi : Prof. Dr. Şimşek Demir

Nisan 2019, 80 sayfa

Elektro-Patlayıcı Detonatörler (EPD) çoğu patlayıcı sistemin esas tetik mekanizmasıdır. Bu sistemlerdeki patlama EPD'deki köprü telinin aşırı akım sonucu yanmasıyla başlar. Bu yanmayı diğer büyük miktardaki patlayıcıların patlaması patlaması takip eder. Bu patlayıcıların kazara veya bilerek patlatılması büyük kayıplara yol açmaktadır. EPD'lerin mikrodalga frekanslardaki elektriksel özellikleri modellenmiş olmakla birlikte, RF imza ile tespit edilmeleri yönünde bir çalışma bulunmamaktadır. Bu amaçla Çoklu Sinyal Sınıflandırma (MUSIC) ve Prony'nin yöntemi kullanılmış ve kullanılan metodların doğruluğunu kanıtlamak için ölçümler yapılmıştır. Bir Çoklu Giriş Çoklu Çıkış (ÇGÇÇ) ölçüm sistemi de kurulmuş ve istatistiksel ÇGÇÇ uygulamasıyla tespit performansında iyileştirme başarılmıştır.

Anahtar Kelimeler: Tespit, RF imza, MUSIC Metodu, Prony'nin Metodu, ÇGÇÇ

To My Family

ACKNOWLEDGMENTS

I wish to express my deepest gratitude to my supervisor Prof. Dr. Şimşek Demir and Prof. Dr. Sencer Koç for their guidance, advice, criticism, and encouragements throughout the research.

I would like to thank Enis Kobal for his supports, Ahmet Önal and Tuğba Aksu for their valuable encouragements.

Lastly, I owe spacial thanks to my family members Hakkı Andaç, Özge Bade, and Orhan Utku Kılıç; this study was meaningless without them.

TABLE OF CONTENTS

LIST OF TABLES

TABLES

LIST OF FIGURES

FIGURES

LIST OF ABBREVIATIONS

ABBREVIATIONS

AR	Auto Regressive
CRN	Centralized Radar Network
CZT	Chirp Z-Transform
DFT	Discrete Fourier Transform
DoA	Direction of Arrival
DRHA	Double Ridged Horn Antenna
DRN	Decentralized Radar Network
EED	Electro-Explosive Detonator
EM	Electromagnetic
ERP	Effective Radiated Power
FAR	False Alarm Rate
FFT	Fast Fourier Transform
ICZT	Inverse Chirp Z-Transform
IDFT	Inverse DFT
IED	Improvised Explosive Devices
LTSI	Late Time Start Index
MA	Moving Average
MIMO	Multiple Input Multiple Output
MSM	MUSIC Spectrum Matrix
MPM	Matrix Pencil Method
MUSIC	Multiple Signal Classification
PSD	Power Spectral Density
PSM	Prony's Spectrum Matrix
RCS	Radar Cross Section
SAR	Synthetic Aperture Radar

SEM	Singularity Expansion Method
SLL	Side Lobe Level
SMA	Sub-Miniature version A
SNCR	Signal to Noise and Clutter Ratio
VNA	Vector Network Analyzer

CHAPTER 1

INTRODUCTION

Frequent use of Improvised Explosive Devices (IED) affects the public safety in rural areas and even in urban public areas where the target of interest in both cases are either innocent, non-politic people or the military forces in duty. A global sensitivity has occurred in terms of the detection of the IEDs. There is an essence need for the detection of the IEDs that are placed in urbanized terrain and public areas.

The detection of the IEDs may be in terms of the structural chemical properties of the explosives included in IED or from the electromagnetic (EM) spectrum of the radar returns. The explosives in the IED may change; however it is observed that the detonator used in the IED is widely an electrically actuated detonator; an electro-explosive detonator (EED) and the EM returns from this device can be modeled. This thesis focuses on the detection of an EED from its EM scattered fields when exposed to EM radiation.

EM modeling of the EED is also given for a practical EED. Electromagnetic properties of EEDs have been investigated due to the unexpected explosions of these trigger mechanisms in the fields with radiators. It was expected that the EEDs have a naturally selective frequency response. This led the researchers to the EM modeling of detonators in order to specify the frequencies which can detonate the device accidentally. However, the detection of the EED based on the complex frequency response has not been studied yet.

On the other hand, comprehensive studies have been conducted in the area of noncooperative target recognition. Noncooperative target recognition stands for the recognition of the target by its inherent properties without cooperating with the target. It can be used for the classification and/or the identification of the target.

MUSIC method and Prony's method are adopted for extracting the complex frequency spectrum of the modeled EED, and it is shown that good agreement between the measured and extracted frequency spectrums is obtained. Adopted MUSIC and Prony's methods are used for the detection of the EED. Experimental detection and false alarm performance for a set of scatterers is studied. Multiple Input Multiple Output (MIMO) measurements are used for detection enhancement purposes.

A literature review is given in Chapter 2 for the noncooperative target detection in the resonance region. The details of the candidate target detection methods, their application areas, advantages and disadvantages are also presented in this chapter. The applied detection methods and the selection criteria are also introduced in this chapter.

In Chapter 3, the details of the applied detection methods are presented. The critical parameters of the methods, determination steps of these parameters, and preliminary results showing the application of the methods are presented. The detection and false alarm properties for a set of resembling-spectrum targets is presented.

In Chapter 4, a MIMO measurement system is introduced. A statistical MIMO approach is adopted for enhancing the detection performance and taking the advantage of the sparse Radar Cross Section (RCS) diversity gain. Detection and False Alarm properties of the proposed methods with the statistical MIMO processing are explored and discussed.

Conclusions and Future Work Chapter gives the conclusions on the presented methods and possible application areas. Noncooperative target detection, recognition, and

classification topics are appealing for various application areas. Future work based on enhancing the detection performance and reducing the computational cost is also given in this chapter.

CHAPTER 2

LITERATURE REVIEW ON TARGET DETECTION METHODS

Electromagnetic detection of targets has been studied for decades. It has been shown that the scattered response of a target can be written as the sum of complex exponentials which is commonly referred to as the Singularity Expansion Method (SEM) [1]-[5]. SEM is a powerful method in terms of the recognition of the scattered response from a target which is evaluated at the late time of the scattered response where the transient scattering from the object has finished, and the steady-state response is obtained. The late time response of a scatterer is validated in the resonance region of the frequency spectrum where the dimension of the object is in the same order of the wavelength associated to the excitation signal. Hence, the time response of the scattered field can be written as the finite sum of exponentials [1]-[5]:

$$z(n) = \sum_{i=1}^{P} c_i e^{s_i n}, \qquad n = 1, \dots, P. \tag{2.1}$$

where s_i are the poles, c_i are the residues of the scattered response, and P is the number of poles. Using SEM approach, one can use different target detection algorithms such as, E-pulse, S-pulse, matrix-pencil method, MUSIC, Prony's method etc. [1]-[9]. In these methods, different approaches are adopted in order to find the poles of the scattered response. However, speaking of the detection of a target with multiple poles; finding the poles of the system is not a practical approach. Instead, focusing on a

method that uses the comparison of the complex frequency spectrums of a reference target and the targets to be compared is a more practical goal.

Brief descriptions of the above mentioned methods are given in this chapter with the indication of the positive and negative aspects of the method.

2.1. Prony's Method

It is convenient to introduce the target detection and recognition methods starting with the Prony's Method. It is the most basic method of all the detection and signal processing algorithms formulated as below for an Auto-Regressive (AR) system model:

$$\frac{X(s)}{W(s)} = H(s) = \frac{b_0}{1+\sum_{k=1}^{P} a_p[k]s^{-k}} \quad \text{where} \quad s = e^{\alpha+j\omega} \tag{2.2}$$

where $W(s)$, $X(s)$, and $H(s)$ are the white noise input, output, and system responses respectively in the complex frequency domain. s^{-k} and $a_p[k]$ are the poles and the residues of the system respectively, and b_0 is the zero order Moving Average (MA) residue. One can easily result with the famous Yule-Walker Equation [10]-[11]:

$$r_x[k] + \sum_{l=1}^{P} a_p(l)r_x[k-l] = |b_0|^2\sigma_w^2\delta[k] \tag{2.3}$$

where $\sigma_w^2\delta[k]$ is the autocorrelation of the white noise input $w[k]$. σ_w^2 the power of the noise and $\delta[k]$ the Delta-Dirac function:

$$\begin{cases} \delta[k] = 1 & if\ k = 0 \\ \delta[k] = 0 & else \end{cases} \tag{2.4}$$

6

$r_x[k]$ is the autocorrelation of the output signal $x[k]$. Writing the Yule-Walker Equation in matrix form:

$$\begin{bmatrix} r_x(0) & r_x(-1) & \cdots & r_x(-P) \\ r_x(1) & \ddots & & \\ \vdots & & & \\ r_x(P) & & & r_x(0) \end{bmatrix} \begin{bmatrix} 1 \\ a_p(1) \\ \vdots \\ a_p(p) \end{bmatrix} = \begin{bmatrix} |b_0^2|\sigma_\omega^2 \\ 0 \\ \vdots \\ 0 \end{bmatrix} \tag{2.5}$$

Eliminating the first row for the above total equation, it reduces to

$$\begin{bmatrix} r_x(0) & r_x(-1) & \cdots & r_x(-P+1) \\ r_x(1) & \ddots & & \\ \vdots & & & \\ r_x(P-1) & & & r_x(0) \end{bmatrix} \begin{bmatrix} a_p(1) \\ a_p(2) \\ \vdots \\ a_p(P) \end{bmatrix} = \begin{bmatrix} r_x(1) \\ r_x(2) \\ \vdots \\ r_x(P) \end{bmatrix}; \quad \boldsymbol{R}\boldsymbol{a_p} = \boldsymbol{r} \tag{2.6}$$

Prony's method solves the least squares solution to the above problem [11]:

$$\boldsymbol{a_p^{LS}} = -(\boldsymbol{R^H R})^{-1}\boldsymbol{R^H r} \tag{2.7}$$

where $\boldsymbol{R^H}$ is the hermitian of $\boldsymbol{R}$, and $(.)^{-1}$ is the matrix inverse operation. Having determined the residues of the AR system model; one can conclude with the poles of the system from the peaks of the fractional (2.2).

It can be seen from the previous work that the Prony's method was mainly adopted for the pole and residue extraction of basic objects such as spheres, thin cylinders whose scattered field is theoretically available [4]-[8]. It is also used for the complex natural resonance extraction in more complex buried unexploded ordnance identification cases [9].

In terms of detection, finding the poles and residues of a target is not practical. Hence, the usage of Prony's Method as in the literature is not advantageous. Prony's method is based on the uniformly sampled sinusoidal signals; which is the main disadvantage for targets with non-periodic scattered response.

2.2. E-Pulse Method

E-pulse Method; named as the abbreviation to the Extinction-Pulse (sometimes also referred to as the Kill-Pulse) is based on the formation of a pulse to kill the scattered response from the target-of-interest in the late-time. SEM equivalent signal representation of the scattered response can be given as:

$$z(t) = \sum_{i=1}^{P} b_i e^{s_i t}, \quad 0 \leq t \leq T_y \tag{2.8}$$

Hence, the convolution of $z(t)$ and the E-pulse $e(t)$ results with zero in the late time:

$$c(t) = z(t) * e(t) = 0 \quad for \quad T_E \leq t \leq T_y \tag{2.9}$$

where '∗' stands for the convolution operator. It is shown in [14] that $E(s)$ has to have zeros identical to the poles of $Y(s)$. There may exist infinite numbers of $e(t)$; we may write the discretized $e(t)$ as:

$$e(t) = \sum_{n=0}^{M} e_n h(t - nT) = \sum_{n=0}^{M} e_n \delta(t - nT) * h(t) \tag{2.10}$$

where $h(t) = 0$ for $t < 0$ & $t > T_h$; $PT + T_h = T_E$

Putting (2.10) in (2.9):

$$c(t) = \sum_{n=0}^{M} e_n z_n(t) = 0 \quad T_E \leq t \leq T_y$$

$$\text{where } z_n(t) = \delta(t - nT) * \left(h(t) * z(t) \right) \; ; \qquad (2.\,11)$$

$$[z_0(t) \ldots z_{M-1}(t)\,] \begin{bmatrix} e_0 \\ \vdots \\ e_{M-1} \end{bmatrix} = -\boldsymbol{e_M z_M(t)}$$

The E-pulse method is basically set on the determination of a finite duration $e(t)$; composed of basis functions $h(t)$; whose convolution with the target response $y(t)$ results with $c(t) = 0$ in the late time of the target response.

The method is verified with various targets [12]-[17] with the a priori information of the number of target poles. However, it is obvious that the number of target poles may not be usually present. Hence, some other studies [18]-[19] focused on determining the number of poles by adaptively minimizing the residue term $\tilde{c}(t)$ in the late time which must be ideally zero (2.9). Later, different performance criteria are also adopted for the E-pulse technique [19]-[21] but none of them is widely recognized.

Additional effort for upgrading the performance has been made in the E–pulse method [19], [22]-[23]. The performance of the method is proven to be improved with higher order basis pulses; quadratic and linear; as a competitive to the first claimed rectangular basis pulse [22]. Multi-directional measurement data is used in [23] for performance upgrade with the claim that the aspect dependent residues may degrade the expected performance of the aspect independent poles. The most impressive upgrade is given in [24] with the evaluation of the early-time response in addition to the late-time response. It is stated that the dimensions of the confusing objects may deteriorate the performance of the method in late time. Hence, the response of the reference target must be compared with candidate targets in both the late-time and

early-time. The upgrade in the performance is given by exact numerical values in a 'Confusion Matrix'.

Evaluating the E-pulse method; it is an effective method in terms of pole extraction. However; its performance is mainly dependent on the appropriate solution of the matrix equation in (2. 10). It can be easily shown that applying Least-Squares solution to this matrix equation; E-pulse method turns out to be a sampled and smoothened version of Prony's Method [25]. The choice of M in (2. 10) may be $M = P$ (forced E-pulse) or $M > P$ (natural E-pulse) in this manner; the performance of the method bounded by the Prony's method in terms of the solution of (2. 11).

2.3. S-Pulse Method

S-pulse method is similar to the E-pulse method in the sense that the S-pulse is an annihilator pulse [26]. However, S-pulse annihilator is designed as a filter $s_i(t)$; which has null energy at all the natural frequencies of the target except the ith one:

$$S^i(s_n) = S^i(s_n^*) = 0 \quad for \quad n = 1, \ldots P, n \neq i \tag{2. 12}$$

where $S^i(s_n)$ is the Laplace Transform of $s_i(t)$, $s_n = \sigma_n + j\omega_n$, and s_n^* is the complex conjugate of s_n. Eq. (2. 9) in E-pulse is modified as follows:

$$c_i(t) = z(t) * s_i(t) = b_i e^{\sigma_i t} \cos(\omega_i t + \psi_i) \quad for \quad i = 1, \ldots P. \tag{2. 13}$$

2.4. Matrix-Pencil Method

Matrix Pencil Method (MPM) is very similar to the Prony's Method, it addresses the poles of (2. 8) by making use of the sampled data in the form:

$$Z = \begin{bmatrix} z(0) & z(1) & \dots & z(P-1) \\ z(1) & \ddots & & \\ \vdots & & & \\ z(M-P) & & & z(M-1) \end{bmatrix} \qquad (2.\,14)$$

Matrices Z_2 and Z_1 are formed by taking out the first and last row of the matrix Z respectively. Decomposing Z_2, Z_1 and analyzing $Z_2 - \lambda\, Z_1$; it can be concluded that:

$$[Z_2^+ Z_1 - z_i I]\, r_i = 0 \qquad (2.\,15)$$

The matrix Z_2^+ is the Moore-Penrose pseudo-inverse of Z_2. Once the eigenvalue estimates z_i are known, the natural frequency estimates may be found via $z_i = e^{s_i \Delta t}$. MPM is usually used for pole extraction [27]-[30]. Reconstruction of the scattered field is also conducted with MPM [29], [31]; and further automatic target classification problems are rarely handled [31]. Apart from these; time-frequency plots have been studied which seem promising in terms of low pole number targets [32].

2.5. Multiple Signal Classification (MUSIC) Method

It has been seen in the previous sections that using the SEM approach, successful results can be obtained in terms of detection with the use of various methods. In this section, we will focus on the application of MUSIC method to the target detection problem. MUSIC method is commonly used in the Direction of Arrival problems [33]-[43] in which the existence of the target is known a priori. However, in this section the focus will be on the use of MUSIC method with detection purposes. (2. 1) can be expanded as (2. 16) where s_i are the poles, and c_i are the residues of the target scattered response and $w(n)$ is the white noise.

$$z(n) = x(n) + w(n) = \sum_{i=1}^{P} c_i e^{s_i n} + w(n), \qquad n = 1, \ldots, N \qquad (2.\,16)$$

$x(n)$ represents the ideal signal with P poles, and $w(n)$ represents the zero-mean Gaussian Noise. The method relies on the fact that the ideal signal $x(n)$ and noise $w(n)$ are uncorrelated. By using the fact that the signal and noise are uncorrelated, the covariance matrix $\boldsymbol{IR}$ can be written as the sum of the signal and noise covariance matrices (2.\,17) & (2.\,18).

$$\boldsymbol{IR} = \boldsymbol{ACA}^H + \sigma^2 \boldsymbol{I}_{N \times N} \qquad (2.\,17)$$

where $\boldsymbol{A} = [a(s_1)\ a(s_2)\ \ldots\ a(s_P)]\quad with$

$$a(s) = \frac{[1\quad e^{-s}\quad \ldots\quad e^{-s(m-1)}]^T}{norm[1\quad e^{-s}\quad \ldots\quad e^{-s(m-1)}]^T}$$

$$\boldsymbol{C} = E\{\boldsymbol{cc}^H\} = E\left\{ \begin{bmatrix} c_1 e^{s_1 n} \\ c_2 e^{s_2 n} \\ \vdots \\ c_L e^{s_P n} \end{bmatrix} [c_1 e^{s_1 n} \quad c_2 e^{s_2 n} \quad \ldots \quad c_L e^{s_P n}] \right\} \qquad (2.\,18)$$

$$= \begin{bmatrix} m_1 & 0 & \ldots & 0 \\ 0 & m_2 & \ldots & \vdots \\ \vdots & \vdots & \ddots & \vdots \\ 0 & \ldots & \ldots & m_P \end{bmatrix}$$

Let $\lambda_1 > \lambda_2 > \cdots > \lambda_P > \lambda_{P+1} > \cdots > \lambda_m$ be the eigenvalues of the covariance matrix $\boldsymbol{IR}$. Let the $e_1, e_2, \ldots, e_P$ be an orthonormal set of eigenvectors associated with the eigenvalues $\lambda_1, \lambda_2, \ldots, \lambda_P$ and $\boldsymbol{G} = [\boldsymbol{e_{P+1}}, \ldots, \boldsymbol{e_m}]$ be a set of orthonormal eigenvectors associated with the eigenvalues $\lambda_{P+1}, \ldots, \lambda_m$. $\boldsymbol{ACA}^H$ has P strictly positive eigenvalues, the remaining $m - P$ equal to zero. Hence;

$$\boldsymbol{IR} \times \boldsymbol{G} = \sigma^2 \boldsymbol{G} = \boldsymbol{ACA}^H \boldsymbol{G} + \sigma^2 \boldsymbol{G} \ \Rightarrow \boldsymbol{ACA}^H \boldsymbol{G} = 0 \qquad (2.\,19)$$

12

Knowing that AC has full column rank;

$$A^H G = 0 \qquad (2.\,20)$$

The spectral-MUSIC method searches for the peaks of the MUSIC Spectrum Function; $P_{unnorm}(s)$.

$$P_{unnorm}(s) = \frac{1}{a^H(s)GG^H a(s)} \text{ where } s = \alpha + j\omega \qquad (2.\,21)$$

The peaks of the MUSIC Spectrum Function gives the complex poles of the target response defined in (2. 16). However, determining the poles of the target response is not practical in terms of detection. Instead, MUSIC Spectrum Function is discretized for α and ω in x and y axes; and the resulting MUSIC Spectrum Matrix is compared between the reference target, and the targets to be recognized. The method was first proposed by Seçmen and Sayan, and was successfully applied to the detection of different targets [44]-[49].

SEM method and its practical application in the well-known and proven detection algorithms is summarized in this chapter. The most promising of the above stated methods is the MUSIC method. The adaptation of the MUSIC method in terms of the detection of an EED in a predefined medium will be given in the next chapter. Prony's method is also adapted with the same approach and performance comparison is given.

CHAPTER 3

MUSIC METHOD APPLIED TO THE DETECTION OF AN EED

Having focused on the promising properties of the MUSIC method to the detection of an EED; practical application is given in detail in this chapter. MUSIC Spectrum Function is a function of complex frequency, $s = \alpha + j\omega$. The peaks of the MUSIC Spectrum Function correspond to the poles of the target. However, in terms of detection and classification, determining the poles of the target is not practical. Instead, MUSIC Spectrum Matrix (MSM) is formed by discretizing α & ω [44]. The resulting MSM of the reference target at the correct late time is compared by the MSM of any target. The resemblance between the compared matrices is linked to the correlation of the measured targets. That is, if the correlation between the two matrices is high, then detection occurs. The details are given in this chapter.

This chapter is organized as follows; first the proposed method is verified with the comparison of the theoretical scattered response, then the application of the method to the range detection is given in full detail, later the adaptation of another method is given for comparison purposes, last of all, the Detection and False Alarm definition and results are given in order to fully test the power of the method. The sample EED used in the thesis is named as 'PRF1' and this name is used in the thesis thereafter.

3.1. The Verification of the Method with the Theoretical Scattered Data

In this section, the developed method is compared with the data from the literature. Usually, a conducting sphere is used for the verification of the SEM based methods

due to its available theoretical solution [5]. SEM based methods are valid in the resonance region which is defined for the largest dimension of the scatterer; D as:

$$\frac{\lambda}{10} \le D \le 10\lambda \qquad (3.1)$$

where λ is the free space wavelength at the defined frequency. Given a frequency range; lower and upper frequencies are the restricting factors for the smallest and the largest dimensions, respectively. For a wideband response of 1-12 GHz, $3\ cm \le D \le 25\ cm$ are the limiting dimensions for the scatterer.

Time domain samples are used in the method; hence the frequency response of the conducting sphere should be transformed to the time domain. It may seem practical to use the most common Discrete Fourier Transform (DFT). However, it is more practical to implement the time domain transform in the way that a Vector Network Analyzer does since the theoretical results are usually to be compared with the practical ones. Then, the theoretically obtained frequency response is first filtered with a normal (Gaussian) window, and then Inverse Chirp Z-Transform (ICZT) is applied to the filtered response. Finally, the resulting time domain response is used in the formation of the MSM of a sphere of 1.8 cm in radius.

In order not to impair the integrity of the thesis, theoretical determination of the time-domain scattering from a sphere is given in Appendix A. The related codes are given in Appendix B.

3.1.1. MSM of a Conducting Sphere

Based on the theoretical time scattered fields from a conducting sphere, MSM of the conducting sphere can be determined. MSM is obtained by discretizing α & ω, and writing the MUSIC Spectrum Function; $P_{unnorm}(s)$, $s = \alpha + j\omega$ in two axes. The

16

windowed time domain response in *Figure A. 5.a* is used as the time response. The resulting MSM can be seen in *Figure 3. 1*.
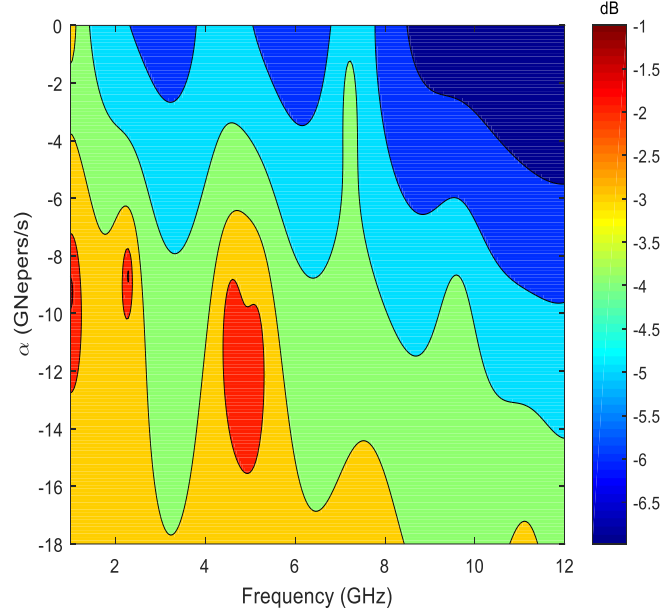
Figure 3. 1. MSM for a 1.8 cm Radius Conducting Sphere

The peaks of the computed MSM is compared by the first two theoretical poles of a perfectly conducting sphere [50]. Pole values are given in Table 3. 1 with an r/c normalization, where r is the radius of the sphere and c is the velocity of light in free space.

Table 3. 1. *Comparison of the Theoretical and Estimated Pole Values by MUSIC Method in*
$$s' = s \times (r/c) \ scale$$

Theoretical pole values [50]	Estimated Pole Values by MUSIC Method
$-0.5 \mp j0.86$	$-0.5256 \mp j0.8791$
$-0.7 \mp j1.81$	$-0.6984 \mp j1.8171$

Estimated values in Table 3. 1 show good resemblance with the theoretical poles. Hence, the verified MSM can be used in the detection of PRF1.

Note: Practically, covariance matrix is calculated in the covariance style which starts the summation from m to N as shown:

$$\widetilde{R} = \frac{1}{N}\sum_{n=m}^{N} y(n)\,y(n)^{H} \qquad (3.\,2)$$

where $y(n)$ column vector is formed by m time samples of the signal, $z(n)$ in (2. 16).

3.2.   The Application of the Method to the Range Detection of PRF1

The MSM method verified in 3.1.1 is used for the detection purposes of PRF1 with practical measurements. Time domain responses of PRF1, medium and other potential scatterers are carried out in two different mediums; anechoic chamber, and echoic medium. The proposed method, applied to both measurements is given.

3.2.1. Anechoic Chamber Measurements

The anechoic chamber measurements are carried out in METU Electrical and Electronics Engineering Department, D221. Antennas are placed on one side of the anechoic chamber, and the potential scatterers are placed on the other side of the chamber on a foam stand, in the seat of the transmitter antenna. The antenna and scatterer placements can be seen in *Figure 3. 2*.

3.2.1.1. Measurement Setup

Measurements are carried out with an HP8720D Vector Network Analyzer (VNA) in 1-12 GHz. Frequency range should be able to resolve the desired time resolution, and should cover the frequency poles of the possible target scatterers. The details of the VNA measurement properties can be seen in the anechoic chamber measurement card in Table 3. 2. Additionally, it should be emphasized that the measurement of the medium with no scatterers is saved as the MEMORY TRACE in the VNA, and DATA/MEMORY Math Function is activated at all the measurements.

18

Double ridged horn antennas (DRHA) are used as the transmitting and the receiving antennas due to their proven performance in the 1-12 GHz frequency band. DRHA are linearly polarized wideband antennas for which the preliminary examples are proposed in the 70's [51]; and nowadays commercially available versions can also be found in different frequency bands [52]- [54].

The reflection and coupling properties of the double-ridged horn antennas can be seen in *Figure 3. 3*. It can be observed from *Figure 3. 3* that reflection for both transmit and receive antennas are below -10 dB, and coupling between the antennas is below -30 dB for 1-12 GHz.

Time domain response of a plane reflector scatterer is measured to be at 30.7 ns as can be seen in *Figure 3. 4*, which corresponds to a one-way path of 4.6 meters between the antennas and the scatterer. Time domain transformation of the VNA is applied in the 0-35 ns, which is enough to capture the two-way scattered response.
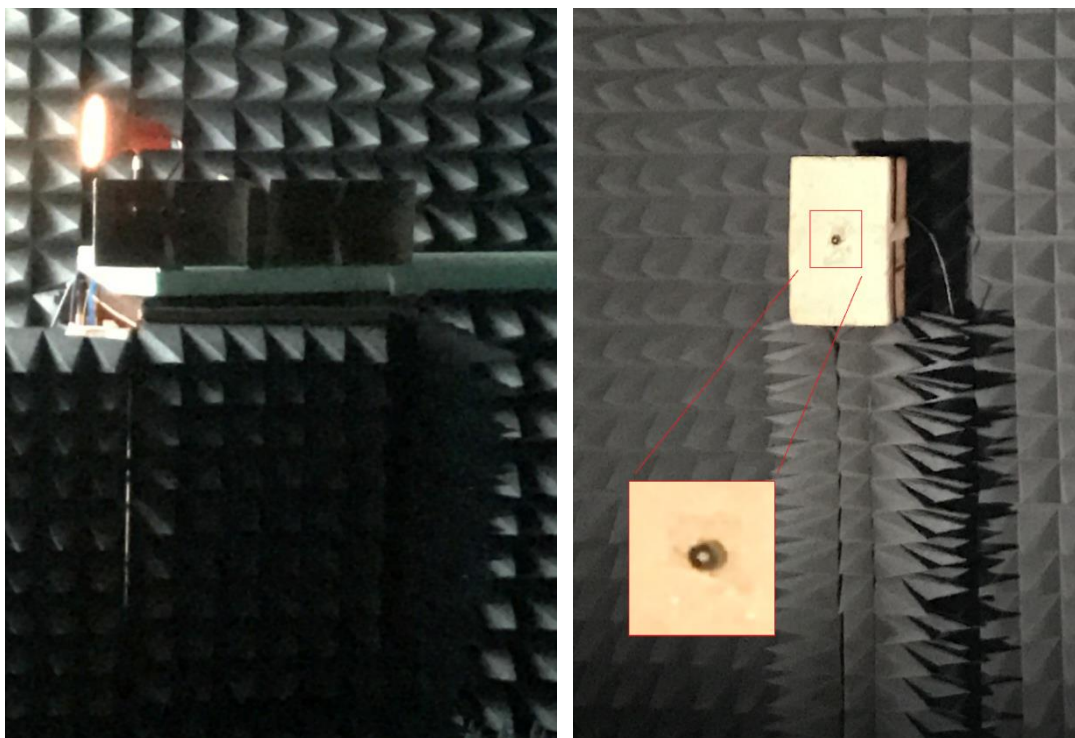
(a)   (b)
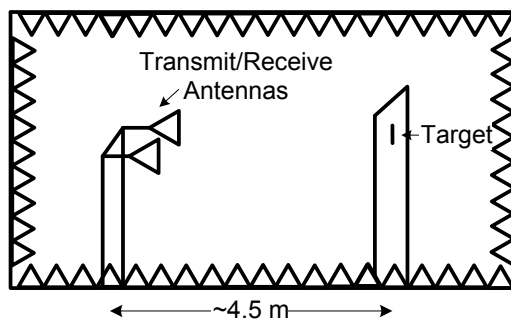
(c)

Figure 3. 2. Measurement Setup in Anechoic Chamber (a) Antennas, (b) Scatterer, (c) Placement of the Elements in Anechoic Chamber

Table 3. 2. *Anechoic Chamber Measurement Card*

Date: 30.01.2017	Place: D221
NA: HP 8720D	Freq: 1-12 GHz
# of points: 1601	Power: 0 dBm
Time Domain Transform: 0-35 ns	
Time Domain Gating: none	
Trace: DATA/MEMORY	
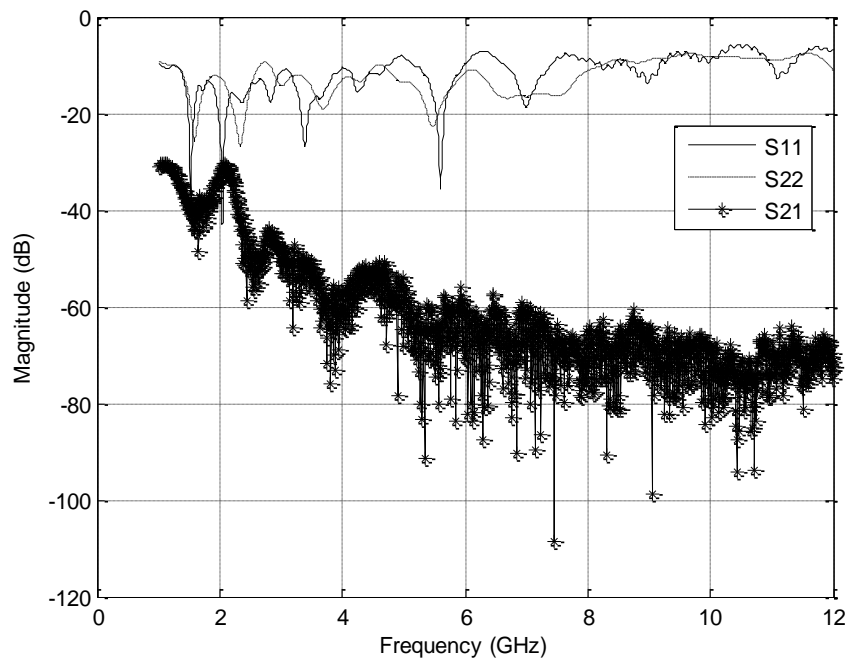
Figure 3. 3. Frequency Domain Response of the Measurement Antennas
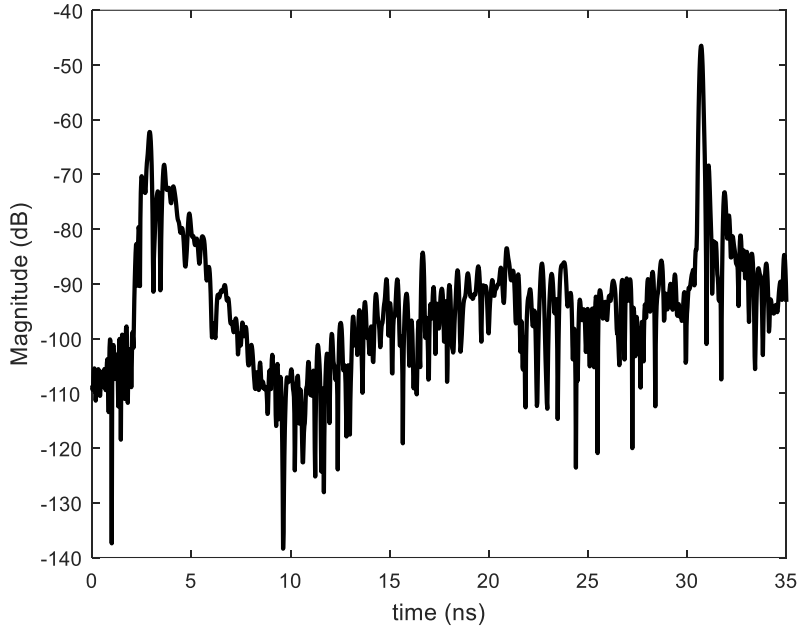
Figure 3. 4. Time Domain Response of the Reflector Scatterer in Anechoic Chamber

3.2.1.2. Application of the Method

Concerning the proposed MUSIC method, the important parameters are:

- P: number of poles
- m: dimension of the covariance matrix $\boldsymbol{IR}$
- N: number of sample points
- T_{sample}: Time domain data sampling period

The selection of P is critical since it reflects the poles of the system; the reduced selection of P would result in performance degradation; whereas the excess selection results in unnecessary excess process time. N and T_{sample} are important since they determine the overall sample length and energy. These values are optimized based on the selection of the highest correlation between the MUSIC Spectrum Matrices (MSM) of the same target. $m = \frac{N}{2}, P = \frac{N}{4}$ is chosen for the best detection performance [59].

22

The determination and optimization of these values are done in the echoic medium, so the details related to the selection of $N = 256$ and $T_{sample} = 5\,ps$ are presented in 3.2.2.

Late Time Start Index (LTSI) is also critical since it determines the correct time interval of the reference target measurement data. Correlation of the MSM's of the reference target is obtained from the same reference late time with incremental start indexes. High correlation is obtained at the correct late time since the poles of the target appear as the peaks of the MSM. Table 3. 3 shows the correlation of the MSM's of two PRF1 measurements with 0.1 ns incremental late time start indexes.

Table 3. 3. *Correlation of MSM Matrices of 'PRF1 vs PRF1' at incremental late time start indexes*

Time Start (ns)	Correlation PRF1 vs PRF1
31.0090	0.5909
31.1090	0.6169
31.2090	0.7707
31.3090	**0.8709**
31.4090	0.8580
31.5090	0.6231
31.6090	0.2612
31.7090	0.4256
31.8090	0.3533
31.9090	0.5306
32.0090	0.6039
32.1090	0.4342
32.2090	0.1708
32.3090	0.3022
32.4090	0.2390

It can be seen from Table 3. 3 that the correlation of the two MSM's is high at 31.309 ns. MSM for PRF1 with 31.309 ns LTSI can be seen in *Figure 3. 5*. It is also wise to check the MSM of the target of interest after the determination of the LTSI.
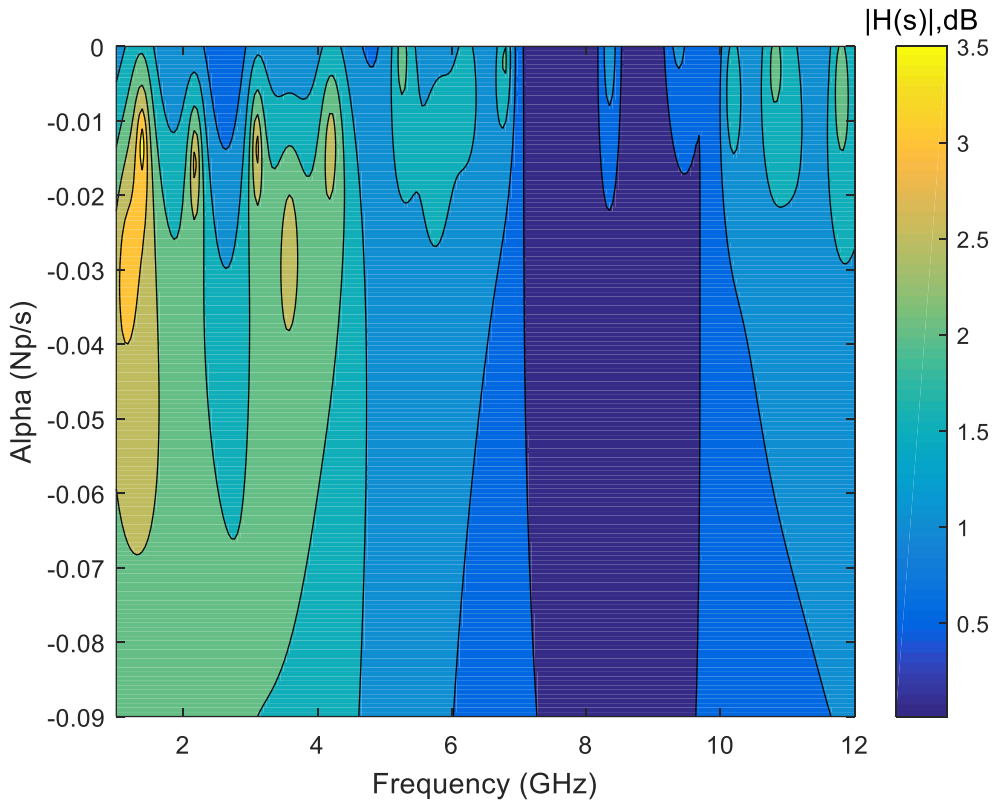
Figure 3. 5. Normalized MSM for PRF1 with 31.309 ns LTSI

Having decided and verified on the LTSI, N, m, p and T_{sample}, the reference data segment for PRF1 can be used for the detection of the target in the range cells of the medium. The measurements for PRF1 and a '1-cm-radius-conducting-sphere' in the 27.322-32.322 ns time interval are used for comparison with the reference PRF1 data. It can be seen from *Figure 3. 6* that the correlation of PRF1 is high with the reference PRF1 data at 31.122 ns which is the position of the target. It can also be observed from *Figure 3. 6* that the correlation of PRF1 with a '1-cm-radius-conducting-sphere' is low in the range; relatively higher at the target position. The relatively higher correlation of PRF1 with the sphere can be explained with the close resonance frequencies of the two target at the 2 GHz-4 GHz frequency range. See *Figure 3. 7* for the MSM of the 1-cm-radius-conducting-sphere.

Based on the preliminary results from the anechoic chamber, it can be stated that the method is promising in terms of the detection of a reference target in the range. It can also be stated that the distinction of the reference target with other scatterers is promising since it resulted in low correlation coefficient with a target of challenging complex spectrum. Now, it is convenient to examine the performance of the method in the echoic medium; i.e. a medium that a scatterer would naturally be included in.
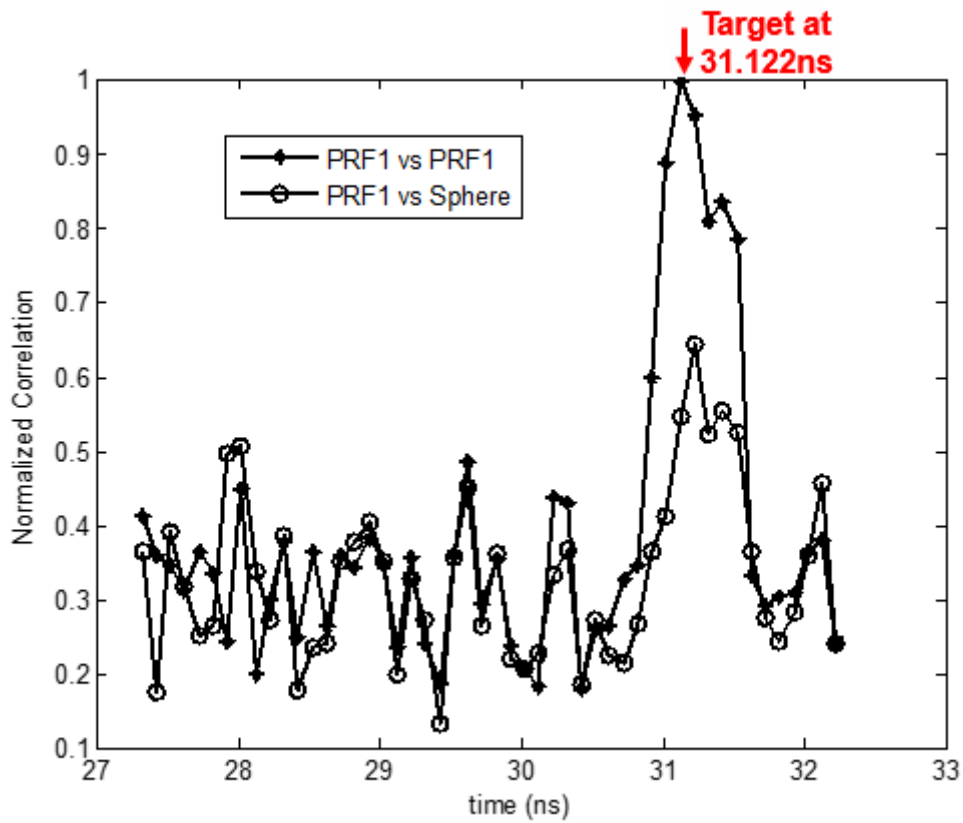
Figure 3. 6. Normalized Correlation of the MSM's of PRF1 vs PRF1 and
1-cm-radius-conducting-sphere

25
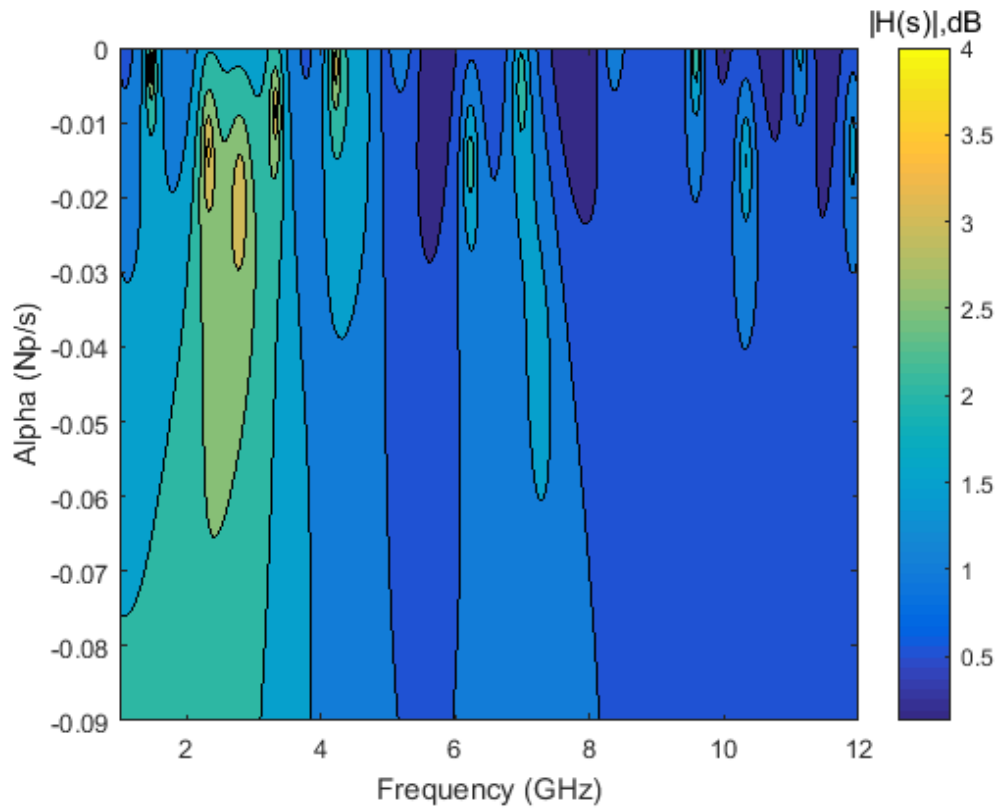
Figure 3. 7. MSM for a 1-cm-radius-conducting-sphere with 31.309 ns LTSI

3.2.2. Echoic Medium Measurements

Anechoic chamber measurement simulates an ideal electromagnetic medium with no scatterers. However, in real life, the environment is surrounded by scatterers, which act as interferers. Indoor mediums pose an additional highly scattering medium with high clutter and multi-path effects from the walls and nearby placed property. It is important for a detection method to be able to cope with the scattering from the environment. Hence, the evaluation of the proposed method is done in the echoic medium.

3.2.2.1. Measurement Setup

Echoic medium measurements are carried out in Ayaslı Research Center of METU Department of Electrical and Electronics Engineering, ARC102. Double-ridged horn antennas are placed on one side of the chamber, and the potential scatterers are placed in front of the antennas, ~90 cm apart. The antenna and scatterer placements can be seen in *Figure 3. 8*. Time domain response of a conducting plane, 'reflector' placed at the reference position of the PRF1 is seen in *Figure 3. 9*. The peak for the 'reflector' is at 8.37 ns; corresponding to a one-way antenna-scatterer path of ~1.25 m distance in air which is compatible with the approximately observed distance.

The measurements are carried out with an E8361A PNA VNA in 1-12 GHz. The details of the VNA measurement properties can be seen in the echoic chamber measurement card in *Figure 3. 8*. Additionally, it should be emphasized that the measurement of the medium with no scatterers is saved as the MEMORY TRACE in the VNA, and DATA/MEMORY Math Function is activated at all the measurements. The reflection and coupling properties of the double-ridged horn antennas can be seen in *Figure 3. 10*.

Figure 3. 8. Antenna and Scatterer Placements in ARC102
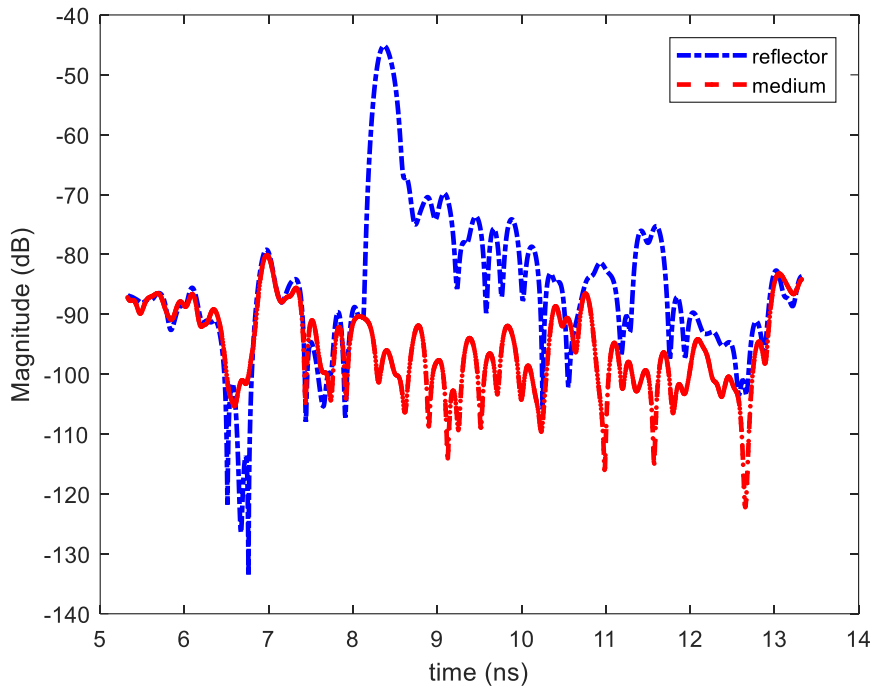
Figure 3. 9. Time Domain Response of the 'reflector' and the 'medium'
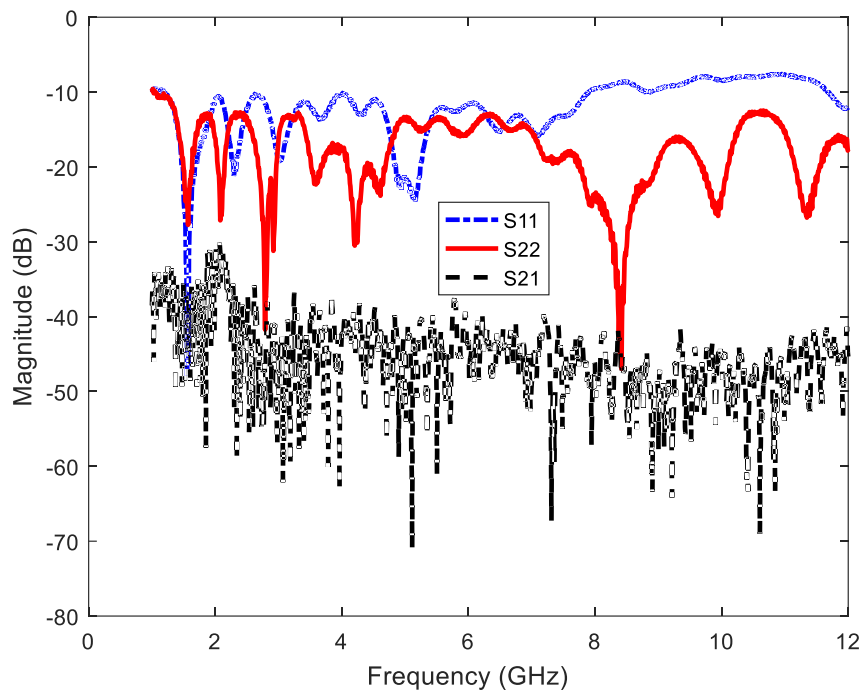
Figure 3. 10. Frequency Domain Response of the Measurement Antennas

29

3.2.2.2. Application of the Method

The selection of N, T_{sample}, and Late Time Start Index (LTSI) values are optimized for the best detection performance. Remember from Section 3.2.1 that $m = \frac{N}{2}$ and $P = \frac{N}{4}$ [59]. Best detection performance is evaluated with the high correlation of the reference target; PRF1; with itself, and low correlation with a totally different scatterer. These criteria make up a 'Detection Factor' that is used to select the most suitable variable set which can be seen in Table 3. 4. The 'Detection Factor' is calculated by subtracting of correlation coefficient of the 'PRF1 vs Medium' from the correlation coefficient of the 'PRF1 vs PRF1' for varying values of N, T_{sample}, and LTSI values as can be seen in Table 3. 4. Note that, throughout the thesis, 'Medium' stands for the measurements of the medium with no scatterers present.

Table 3. 4. *Detection Factor for varying N, resoln and LTSI values*

N	resoln (ps)	LTSI (ns)	PRF1 versus		Detection Factor
			PRF1	Medium	
256	5	8.275	0.3652	0.0313	0.3339
256	5	8.375	0.4178	0.1244	0.2934
256	5	8.475	0.8536	0.303	0.5506
256	5	8.575	0.6084	0.0852	0.5232
256	5	8.675	0.944	0.1491	**0.7949**
256	5	8.775	0.2429	0.0953	0.1476
128	5	8.275	0.2235	0.1643	0.0592
128	5	8.375	0.1883	0.019	0.1693
128	5	8.475	0.8173	0.0498	0.7675
128	5	8.575	0.0999	0.103	-0.0031
128	5	8.675	0.1767	0.2299	-0.0532
128	5	8.775	0.7134	0.1092	0.6042
256	2.5	8.275	0.6493	0.1354	0.5139
256	2.5	8.375	0.844	0.24	0.604
256	2.5	8.475	0.7317	0.0866	0.6451
256	2.5	8.575	0.2831	0.0688	0.2143
256	2.5	8.675	0.8274	0.1434	0.684
256	2.5	8.775	0.7596	0.2896	0.47
128	2.5	8.275	0.5735	0.4293	0.1442
128	2.5	8.375	0.6591	0.251	0.4081
128	2.5	8.475	0.9474	0.3698	0.5776
128	2.5	8.575	0.7868	0.5454	0.2414
128	2.5	8.675	0.5849	0.8149	-0.23
128	2.5	8.775	0.5132	0.1093	0.4039

It can be seen from Table 3. 4 that $N = 256, m = \frac{N}{2} = 128, P = \frac{N}{4} = 64, T_{sample} = 5\ ps$, and LTSI=8.675 ns results in the highest 'Detection Factor'. In addition to the highest value of the 'Detection Factor', the cumulative high value of the 'Detection Factor' at $N = 256, resoln = 5\ ps$ is also an important factor.

Having decided and verified on these values, the reference data segment for PRF1 can be used for the detection of the target in the range cells of the medium. The

measurements for PRF1 and medium, in the 7.5-10.9 ns time interval are used for comparison with the reference PRF1 data. As can be seen from *Figure 3. 11*, the correlation of PRF1 versus PRF1 is high at 8.7 ns as expected; which is the position of PRF1. Additionally, there is a high correlation at 10.5 ns which is a 'False Alarm'. The correlation of PRF1 with the medium is also high at some range points, but is generally low.
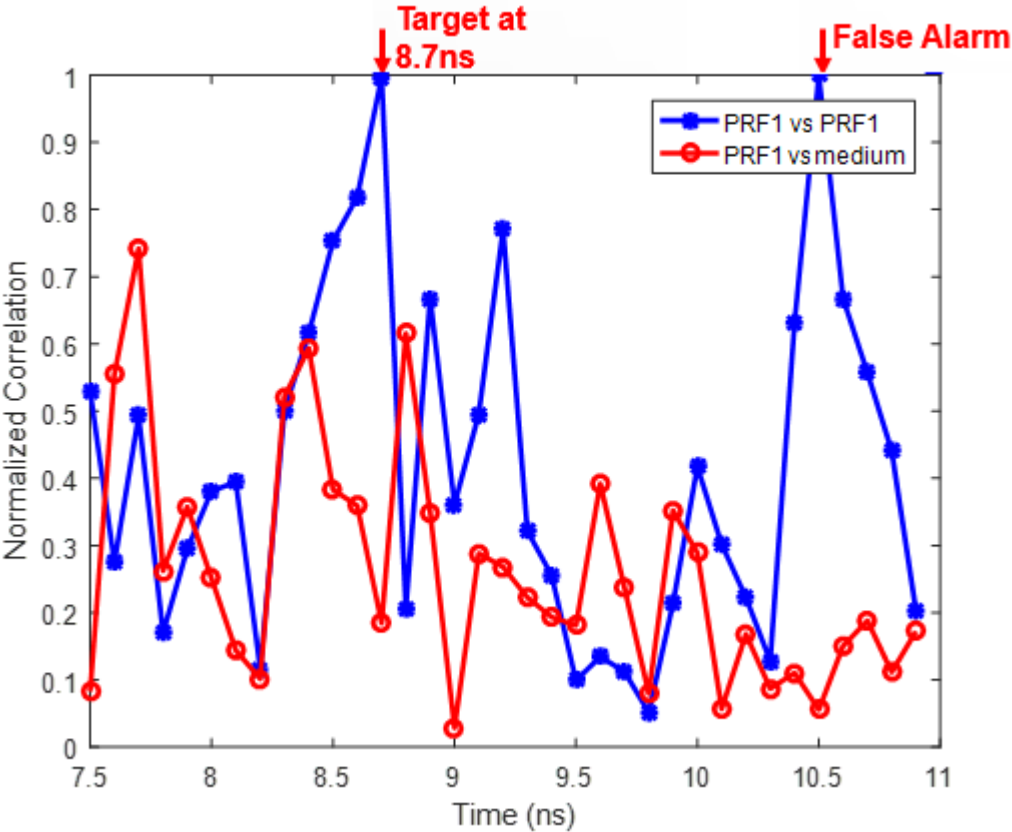
Figure 3. 11. Normalized Correlation of the MSM's of 'PRF1 vs PRF1' and 'PRF1 vs medium'

Observed high correlation values of the medium with the reference data must be handled for lower 'False Alarm' rates. The 0.05 ns shifted samples of the time domain data is input to the detection algorithm and the resulting correlation is averaged with the original one across the time range. The correlation for two single measurements of

32

'PRF1 vs PRF1'; reference and time-shifted, and the averaged correlation can be seen in *Figure 3. 12*. It can be concluded from *Figure 3. 12* that the high correlation values can be lowered as the result of the averaging algorithm. However, it should be noted that the averaging algorithm doubles the computation time by doubling the computation.
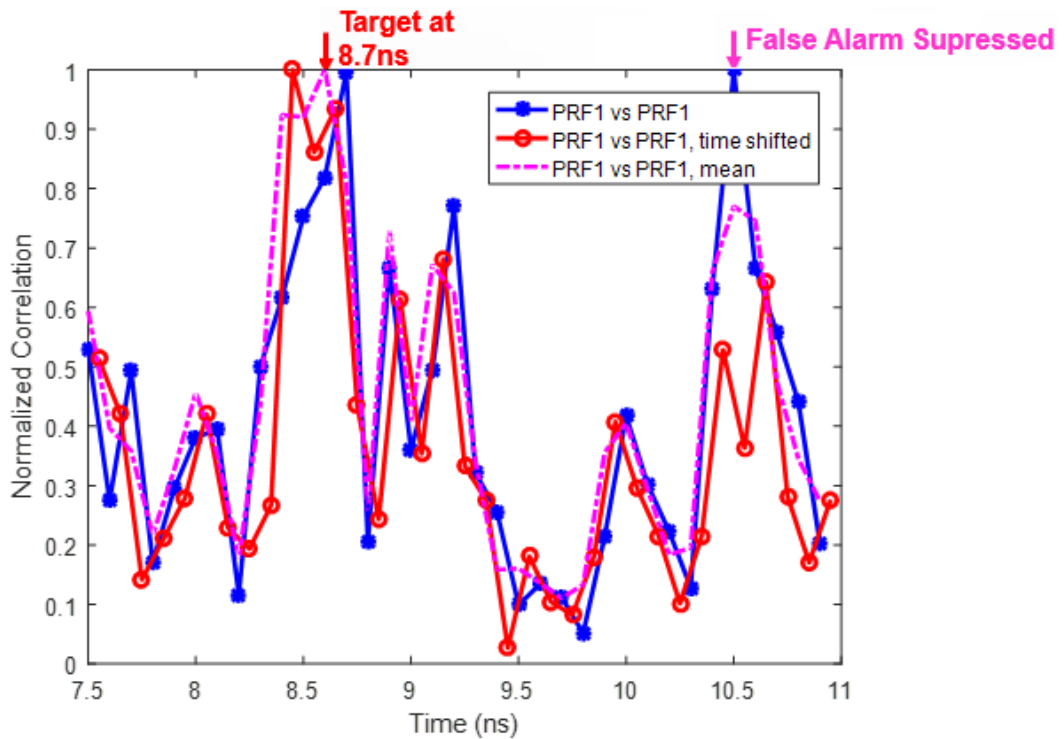
Figure 3. 12. Normalized Correlation of the MSM's of 'PRF1 vs PRF1', Single, Time-Shifted, and Averaged Measurements

In terms of detection in range, a scatterer at a position different than the reference scatterer may also need to be verified. For this purpose, PRF1 is placed at a position ~24 cm apart from its reference position. The correlation of the PRF1 at ~24 cm behind the reference position vs PRF1 in the 7.5-10.9 ns time interval can be seen in *Figure 3. 13*.
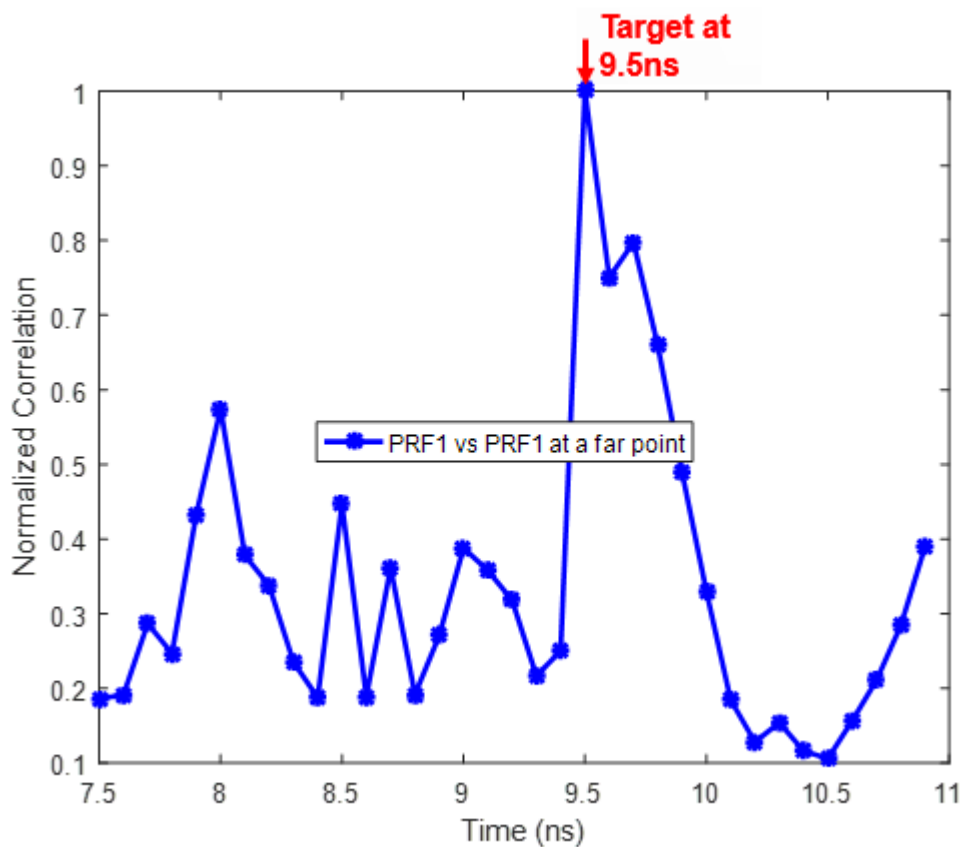
Figure 3. 13. PRF1 vs PRF1 at ~24 cm Behind the Reference Position, Averaged Correlation

It can be seen from *Figure 3. 13* that the correlation is high at 9.5 ns which corresponds to a 0.8 ns further position. Hence, it can be concluded that a target at a point different than the reference position can be detected. Having verified the method both with the theoretical and the measurement data, another method; Prony's method is also adopted in the same manner and the performance is compared at the following chapters.

3.3. Adaptation of Prony's Method

In Chapter 2, it is stated that MUSIC is superior compared to the mentioned methods. It is possible to apply one of the aforementioned methods in terms of a discretized

complex spectrum and compare the results. Prony's Method is adopted for this purpose. Prony's Method is based on an Auto-Regressive (AR) system since:

- Moving average (MA) processes have autocorrelation which are non-linear functions of filter coefficients $b_0, b_1, b_2 \dots$,

- MA processes have deep nulls at the power spectral density (PSD),

- A sufficiently large order of Auto-Regressive (AR) process can approximate any PSD.

In an all-pole system, system response can be modeled as:

$$\frac{X(s)}{W(s)} = H(s) = \frac{b_0}{1 + \sum_{k=1}^{P} a_p[k]s^{-k}} \qquad (3.3)$$

$$x[n] + \sum_{l=1}^{P} a_p(l)x[n-l] = b_0 w[n] \qquad (3.4)$$

for $k \geq 0$

$$E\{x[n]x[n-k]\} + \sum_{l=1}^{P} a_p(l)E\{x[n-l][n-k]\} = b_0 E\{w[n]x[n-k]\} = 0 \qquad (3.5)$$

Hence; this results with the famous Yule-Walker Equation:

$$r_x[k] + \sum_{l=1}^{P} a_p(l)r_x[k-l] = |b_0|^2 \sigma_w^2 \delta[k] \qquad (3.6)$$

Writing the Yule-Walker Equation in matrix form:

$$\begin{bmatrix} r_x(0) & r_x(-1) & \cdots & r_x(-p) \\ r_x(1) & \ddots & & \\ \vdots & & & \\ r_x(p) & & & r_x(0) \end{bmatrix} \begin{bmatrix} 1 \\ a_p(1) \\ \vdots \\ a_p(p) \end{bmatrix} = \begin{bmatrix} |b_0^2|\sigma_\omega^2 \\ 0 \\ \vdots \\ 0 \end{bmatrix} \qquad (3.7)$$

Eliminating the first row for the above total equation, it reduces to

$$\begin{bmatrix} r_x(0) & r_x(-1) & \cdots & r_x(-p+1) \\ r_x(1) & & \ddots & \\ \vdots & & & \\ r_x(p-1) & & & r_x(0) \end{bmatrix} \begin{bmatrix} a_p(1) \\ a_p(2) \\ \vdots \\ a_p(P) \end{bmatrix} = \begin{bmatrix} r_x(1) \\ r_x(2) \\ \vdots \\ r_x(P) \end{bmatrix} ; \qquad Ra_p = r \qquad (3.8)$$

Prony's Method applies the least squares solution to the above problem [11]:

$$a_p^{LS} = -(R^H R)^{-1} R^H r \qquad (3.9)$$

a_p^{LS} is used in Equation (3. 3), and the system response is obtained for the discretized complex frequency; $s = \alpha + j\omega$. The proposed method is applied in two different mediums; anechoic chamber, and echoic medium.

3.3.1. Anechoic Chamber Measurements

The measurement setup and the measured time domain data in 3.2.1 is used in this section. The variables are also preserved; $N = 256, P = 64, T_{sample} = 5\,ps$, and LTSI=31.309 ns. The measurements for PRF1 and a '1-cm-radius-conducting-sphere' in the 27.322-32.322 ns time interval are used for comparison with the reference PRF1 data. The '1-cm-radius-conducting-sphere' used in the measurements is abbreviated as 'Sphere' throughout the thesis. The resulting normalized correlation values of the Prony's Spectrum Matrices (PSM) can be seen in *Figure 3. 14*.

36
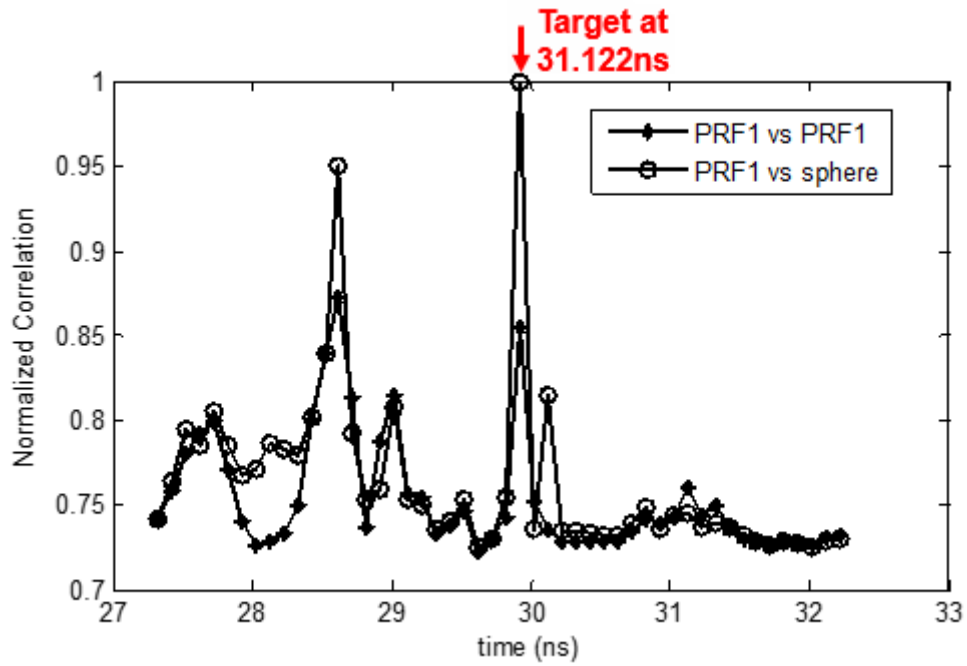
Figure 3. 14. Normalized Correlation of the PSM's of 'PRF1 vs PRF1' and
'PRF1 vs Sphere'

It can be observed from *Figure 3. 14* that there are unexpectedly high correlation
values of 'PRF1 vs Sphere' and 'PRF1 vs PRF1' throughout the range which seem to
shadow the true scatterer response at around 31.3 ns.

3.3.2. Echoic Medium Measurements

The measurement setup and the measured time domain data in 3.2.2 is used in this
section. The variables are also preserved; $N = 256, P = 64, T_{sample} = 5\,ps$, and
LTSI=8.675 ns. The correlation of 'PRF1 vs PRF1' and 'PRF1 vs Medium', in the
7.5-10.9 ns time interval is given *Figure 3. 15*. Despite the expected high correlation
of 'PRF1 vs PRF1' at the reference position; 8.675 ns, it can be observed from *Figure
3. 15* that the correlation of 'PRF1 vs PRF1' is high at 7.7 ns which is a 'False Alarm'.
There are also high correlation values of 'PRF1 vs Medium' at certain time instants
which would potentially result in a 'False Alarm'.
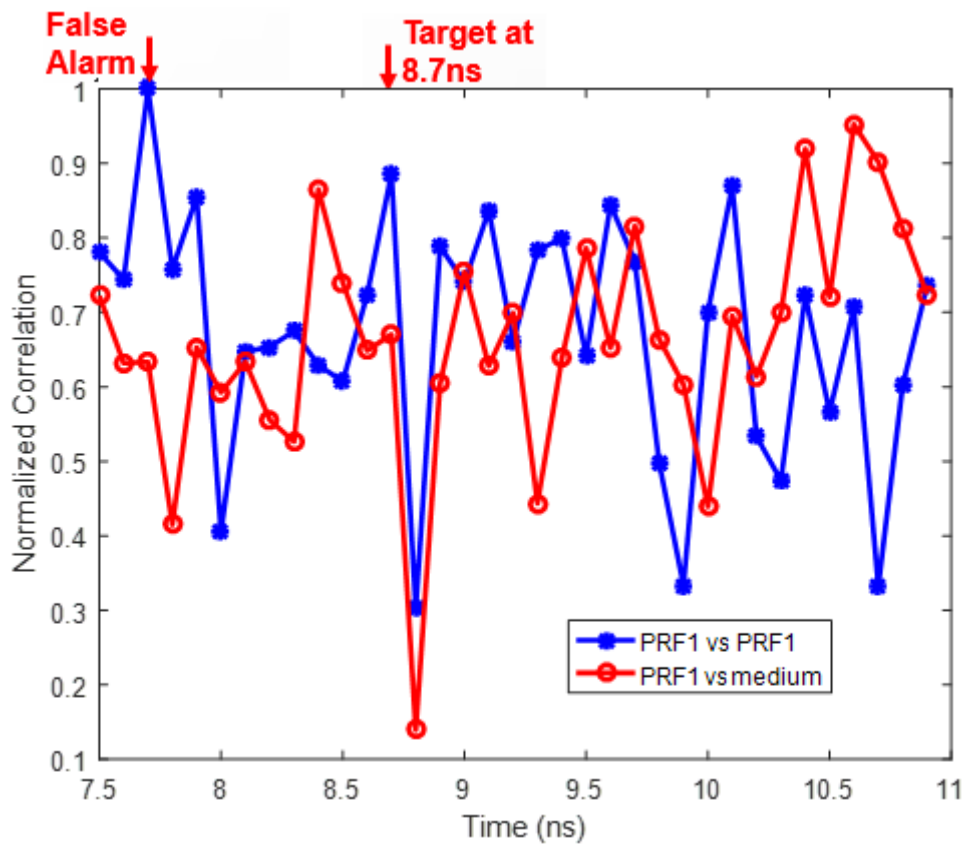
Figure 3. 15. Normalized Correlation of the PSM's of 'PRF1 vs PRF1' and
'PRF1 vs Medium'

In order to handle 'False Alarm' rates, 0.05 ns shifted samples of the time domain data is input to the detection algorithm, and reference, time-shifted, and averaged correlations of the 'PRF1 vs PRF1' can be seen in *Figure 3. 16*. It can be concluded from *Figure 3. 16* that the unexpected high correlation values can be lowered, and the highest peak is obtained at the correct reference time instant, 8.7 ns.
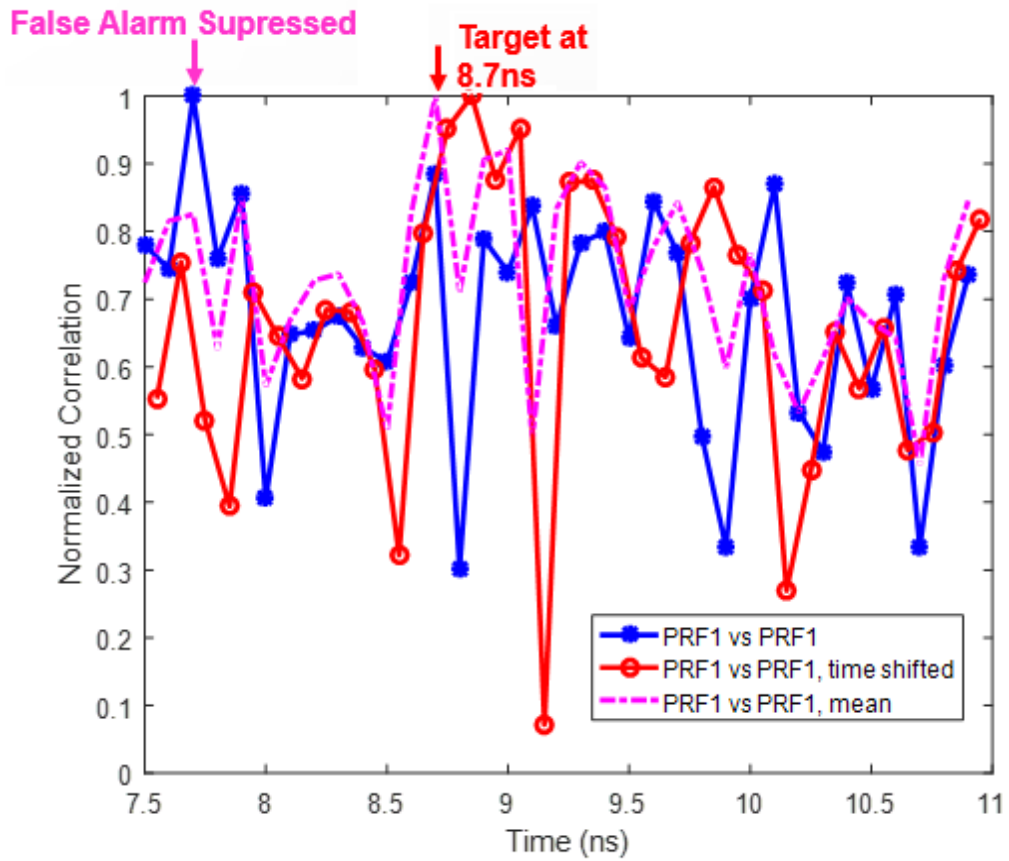
Figure 3. 16. Normalized Correlation of PSM's of 'PRF1 vs PRF1', Single, Time Shifted, and Averaged Measurements

In terms of detection in range, a scatterer at a position different than the reference scatterer may also need to be verified. For this purpose, PRF1 is placed at a position ~24 cm apart from its reference position. The correlation of the PRF1 at ~24 cm behind the reference position vs PRF1 in the 7.5-10.9 ns time interval can be seen in *Figure 3. 17*. The peak response is obtained at 10.8 ns; however there are also relatively high correlation values across the range.
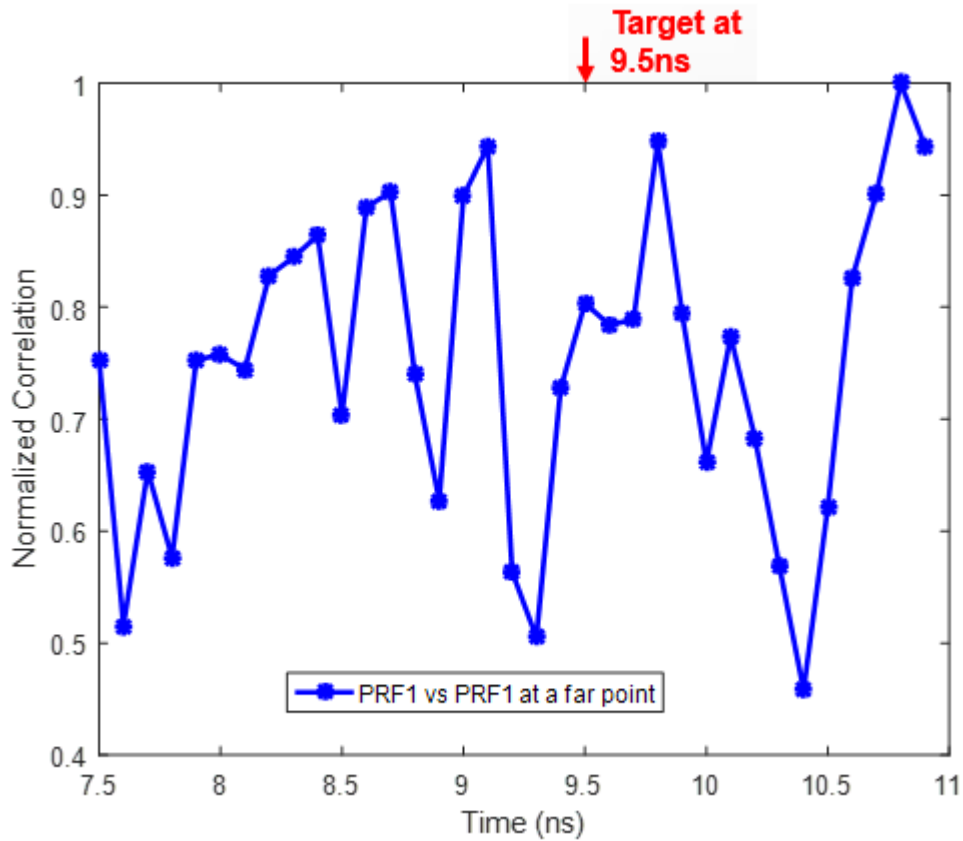
Figure 3. 17. Normalized Correlation of PSM's of 'PRF1 vs PRF1' at ~24 cm Behind the Reference Position

Concerning the proposed methods, the correlation values given in this chapter are exemplary and are not sufficient for making a decision on the performance of the methods. However, they are given to show that the proposed methods are promising. The performance of the proposed methods is evaluated in the next section with the analysis of Detection and False Alarm rates.

While proceeding to the next chapter, it should be emphasized that for lower 'False Alarm' rates, it is decided that averaging the correlation values from the reference and 0.05 ns shifted time samples is a good practice, and is applied in the next chapters.

3.4.   Detection and False Alarm Rates

The proposed detection methods are evaluated by multiple measurements of different scatterers. The decision number out of the total measurement number for each scatterer versus all scatterers is counted. Decision of a scatterer versus itself gives a 'Detection', decision of a scatterer with other scatterers or medium gives a 'False Alarm'. A set of scatterers are examined for their Detection and False Alarm Rates, P_d and P_{fa} respectively.

In our measurements, four different scatterers are used and their detections out of the measurements are presented. These scatterers are: 'PRF1', '1-cm-radius-conducting-sphere', 'GPS Antenna', and an 'open-circuited 18-cm-long two-wire'. This set of scatterers is proposed as a challenging set in terms of the resemblance of the pole positions; then it would be wise to check the MSM for these scatterers. The united pole positions in a single graph can be seen in *Figure 3. 18*. The MSMs of each scatterer can be seen in *Figure 3. 19*. The details related to the measurement setup, and the results for MUSIC and Prony's method are given in the proceeding sections.
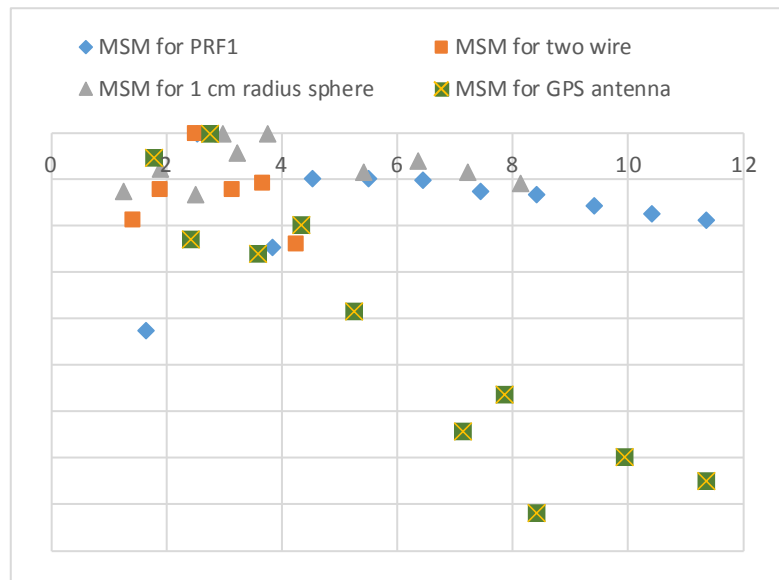
Figure 3. 18. Pole Location of the Scatterers

41
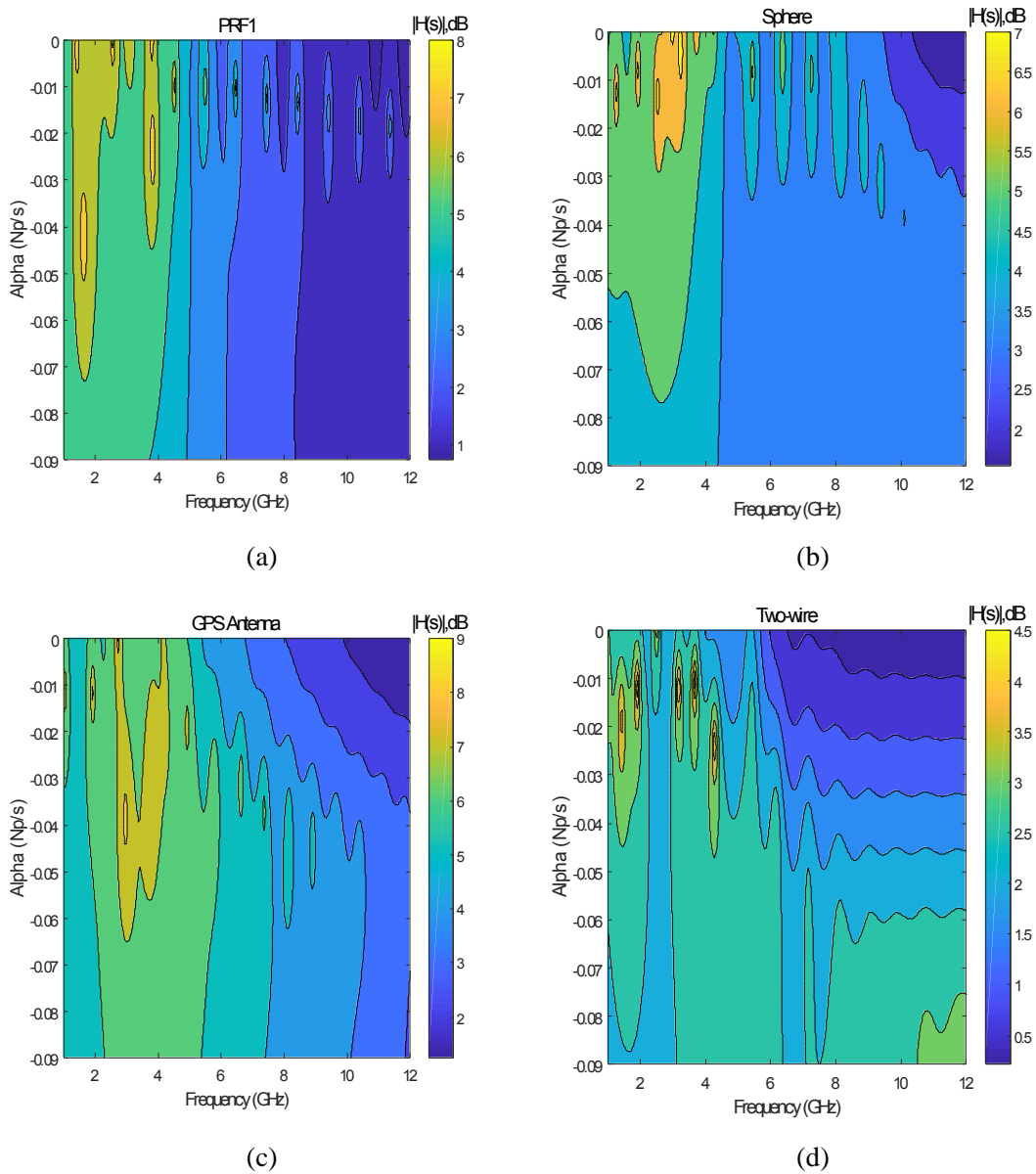
Figure 3. 19. Normalized MSM for (a) PRF1, (b) Sphere, (c) GPS antenna, (d) Two-wire

3.4.1. The Measurement Setup

The measurement setup is the same as Section 3.2.2 except the antennas. Two Vivaldi antennas are preferred in this section. Antenna placement can be seen in *Figure 3. 20*. The details of the VNA measurement properties can be seen in the measurement card

in Table 3. 5. The reflection and coupling properties of the Vivaldi antennas can be seen in *Figure 3. 21*.

Table 3. 5. *Measurement Card*

Date: 10.04.2018	Place: ARC102
NA: E8361A PNA	Freq: 1-12 GHz
# of points: 1601	Power: 0 dBm
Time Domain Transform: 6-14 ns	
Time Domain Gating: None	
Trace: DATA/MEMORY	
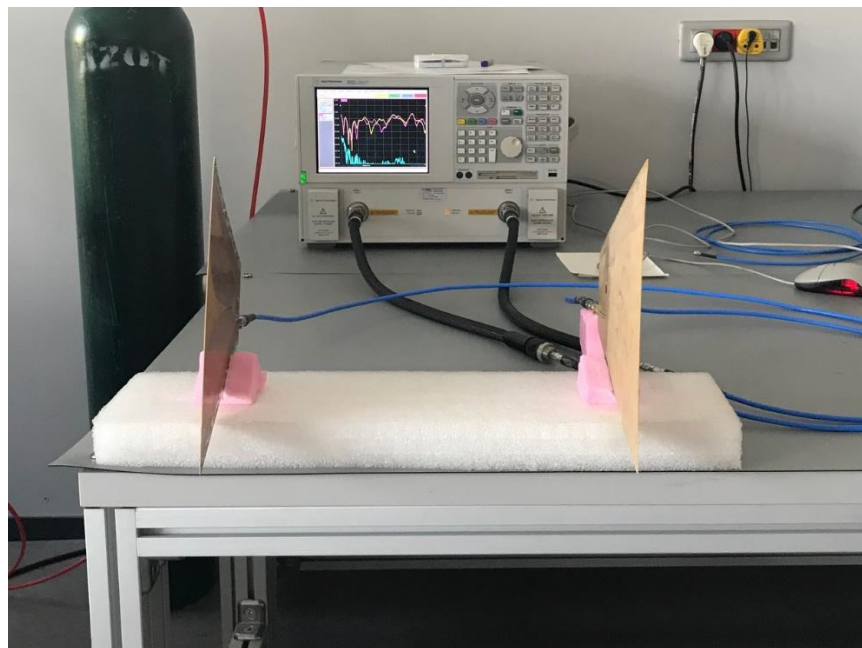
Figure 3. 20. Measurement Setup
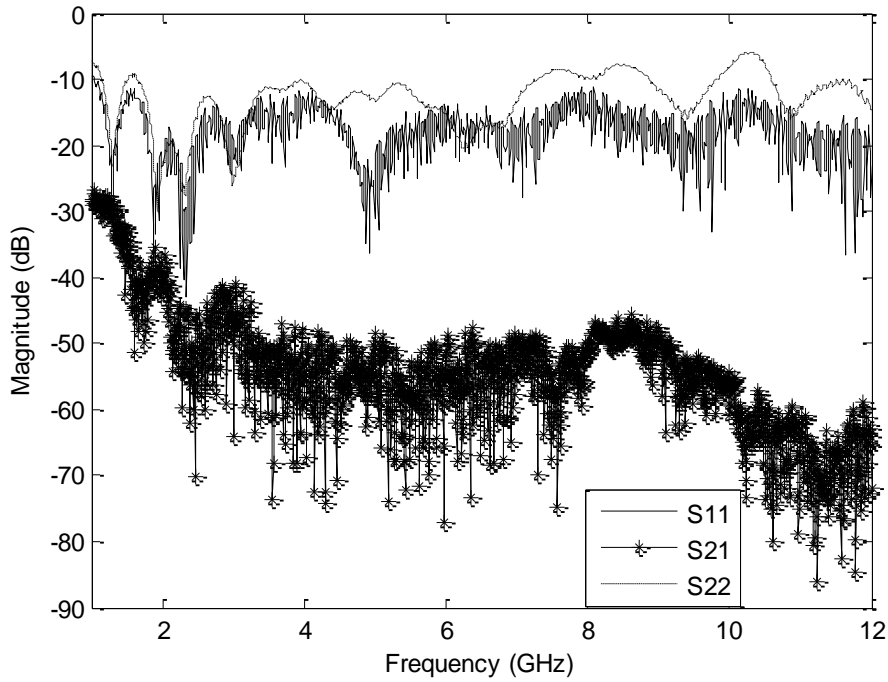
Figure 3. 21. Frequency Domain Response of the Measurement Antennas

3.4.2. MUSIC Method Detection and False Alarm Rates

A total of ten measurements of each scatterer is taken at two range points; five measurements at the reference range point and five measurements at a point ~10 cm behind the reference point. Decision of a scatterer with itself, divided by measurement number (10) gives detection rate, P_d. Decision of a scatterer with other scatterers and medium, divided by measurement number (40) gives false alarm rate, P_{fa}. P_d & P_{fa} are given in Table 3. 6 for each scatterer.

Table 3. 6. *P_d & P_{fa} Matrix for MUSIC Method*

Targets	P_d	P_{fa}
PRF1	0.8	0.35
Sphere	0.6	0.225
GPS Ant.	0.7	0.25
Two Wire	0.5	0.45

3.4.3. Prony's Method Detection and False Alarm Rates

Prony's method is applied to the same measurement data in 3.4.2, and P_d & P_{fa} matrix can be seen in Table 3. 7.

Table 3. 7. *P_d & P_{fa} Matrix for Prony's Method*

Targets	P_d	P_{fa}
PRF1	0.7	0.275
Sphere	0.7	0.325
GPS Ant.	0.9	0.425
Two Wire	0.6	0.075

3.4.4. Comments and Comparison

It can be observed from Table 3. 6 that MUSIC seems to be distinguishing PRF1 with 0.8 detection and 0.35 false alarm. Prony's method, on the other hand, shown in Table 3. 7 that, 0.7 P_d and 0.275 P_{fa} for PRF1. The detection of 'Two Wire' seems possible with Prony's method with 0.6 P_d and 0.075 P_{fa} in contrary to MUSIC method's 0.5 P_d and 0.45 P_{fa}. It can be seen that the performance of the Prony's method is comparable to MUSIC method. The Signal to Noise and Clutter Ratio (SNCR) is ~20 dB for this measurement setup. It is experienced that measurements conducted with a high SNCR value results in comparable performance of the two methods.

In order to enhance the performance of the method and additionally enable the 3D detection in a random medium, Multiple Input Multiple Output (MIMO) sensor placement and processing is necessary. The MIMO measurements and the related results are presented in the next chapter.

CHAPTER 4

MULTIPLE INPUT MULTIPLE OUTPUT (MIMO) MEASUREMENT APPLIED TO THE DETECTION OF PRF1

The radar concepts were appreciated and continued to be developed after World War II. By the advances in computational capabilities after the 1970s, more complicated processing was considered by the system designers. Hence, Multiple-Input Multiple-Output (MIMO) radars have become an active area of research. It is not easy to point to the first example of MIMO radar because different radar types can also be considered as MIMO radars due to their multiple processing properties. For instance, Synthetic Aperture Radar (SAR) or fully polarimetric radar may be interpreted as MIMO radars in terms of the multiple position and polarization measurements respectively.

4.1.   A Review of the MIMO Concept

There are two basic regimes of operation for MIMO radar systems considered in the literature. In the first regime, the transmit array elements (and receive array elements) are broadly spaced, providing independent scattering responses for each antenna pairing, referred to as 'Statistical MIMO radar' [61]. In the second regime, the transmit array elements (and receive array elements) are closely spaced so that the target is in the far field of the transmit-receive array, sometimes referred to as 'Coherent MIMO radar' [62].

The performance of the different forms of MIMO is also investigated in [62] with the usage a constant Effective Radiated Power (ERP) for an objective comparison.

Transmitter-receiver (TX-RX) path pairs are termed 'nodes' and the individual TX-RX pairs are 'device'. The radar networks under investigation are made up of one to five devices exhibiting 1, 4, 9, 16, and 25 nodes, respectively. The signal model in the MIMO system is given in [62]. The brief descriptions of the MIMO's to be compared are given as:

4.1.1. Coherent MIMO

In this approach, the coherent processing of periodical and closely placed transmit-receive array elements are used. In terms of Direction of Arrival (DoA), the theoretical resolution dictated by the transmitted waveform bandwidth is overcome by coherent MIMO [63]-[65].

4.1.2. Statistical MIMO

This type of MIMO radar system exploits measurements of independent samples of target scattering as the basis for improving the probability of detection. Sparse placement of the antennas takes the advantage of exploiting the RCS diversity; thus enhancing the detection capability since over the decade fluctuations in the RCS of a target may be observed [61], [65]-[67].

Data samples may be processed incoherently and in a centralized architecture; that is, there is a central processing unit collecting the receiver outputs from all the nodes and returning a decision about the presence or absence of a target which is called the Centralized Radar Network (CRN).

Alternatively, data samples may be processed in each node and a decision is extracted by the system which is called the Decentralized Radar Network (DRN). This is a two-stage approach to detection which consists of the parts:

1. Detection is extracted from the signals for each node (i.e., in decentralized preprocessing)

2. The decisions are jointly fused, so the system can provide a final output.

The thresholds at all the nodes can be set to different values in order to guarantee the same False Alarm Rate (FAR). After each mono/bistatic decision has been made, a vector v, containing only zeros (i.e., no detections) and ones (i.e., detections), is available for the second stage of processing. At this point the decision rule assumes the target to be present when L elements of the vector are set at (4. 1):

$$\sum_{k=1}^{MN} v[k] \geq 1 \; where \quad MN = \# \; of \; nodes \qquad (4. 1)$$

Incoherent systems have an advantage over coherent systems as they incrase the detection capability. The decentralized radar networks show increased tolerance to jamming without any of the counter measures commonly adopted. These systems have also an advantage over the centralized systems since they require a smaller bandwidth for transmitting the information to the decision unit [62]. Hence, a DRN MIMO approach is adopted for this purpose.

4.2.   Application of the DRN MIMO to the Range Detection

The statistical MIMO approach is adopted for the advantage of processing the scattering of the same scatterer at different aspect angles [61], [65]-[67]. The transmit-receive antenna pairs are placed at three different sparce positions. The H-plane beamwidth of the DRHA, which is the plane of angular diversity is measured. The beamwidth values can be found in Table 4. 1, and the measured H-plane radiation patterns can be seen in *Figure 4. 1*. Measurements are conducted in the Anechoic Chamber Facility of the Department of Electrical and Electronics Engineering, Middle East Technical University, at D-221.

Table 4. 1. *H-plane Beamwidth Values for DRHA*

Frequency	Beamwidth
2 GHz	48.5°
6 GHz	38.2°
9 GHz	33.2°
12 GHz	44.3°
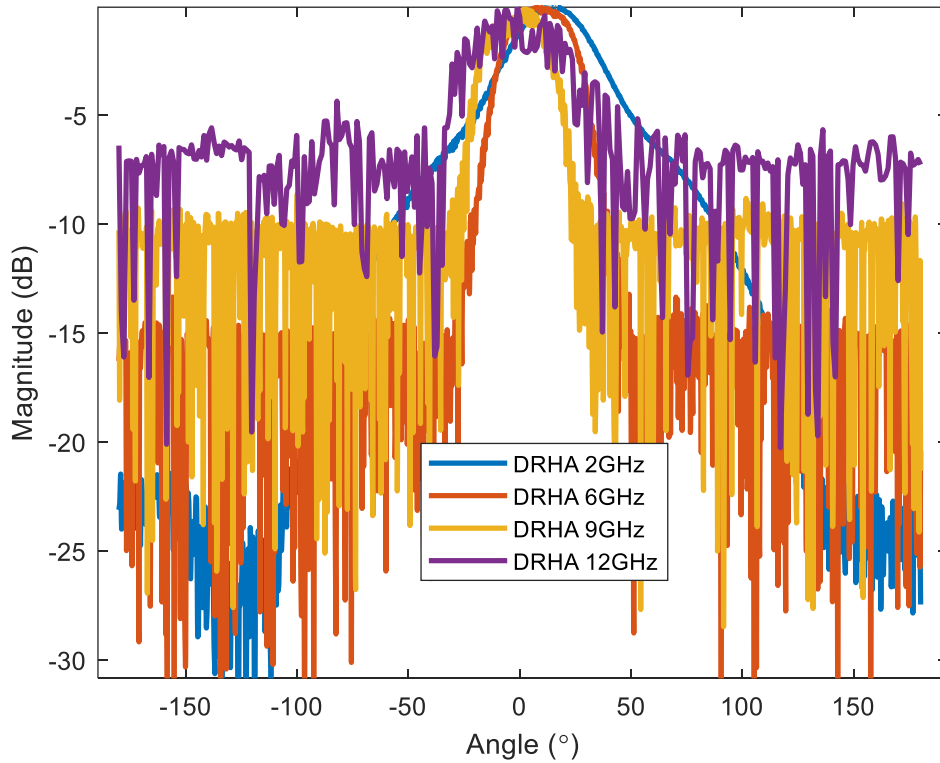
*Figure 4. 1.*H-plane Pattern of the DRHA

In accordance with the measured beamwidth values, transmit-receive antenna pairs are placed at 0° and ±7.5° off the boresight of the antenna. The VNA properties and the measurement setup can be seen in Table 4. 2, and *Figure 4. 2* respectively.

Table 4. 2. *Measurement Card*

Date: 28.01.2019	Place: ARC102
NA: E8361A PNA	Freq: 1-12 GHz
# of points: 1601	Power: 4 dBm
Time Domain Transform: 6-14 ns	
Time Domain Gating: None	
Trace: DATA/MEMORY	
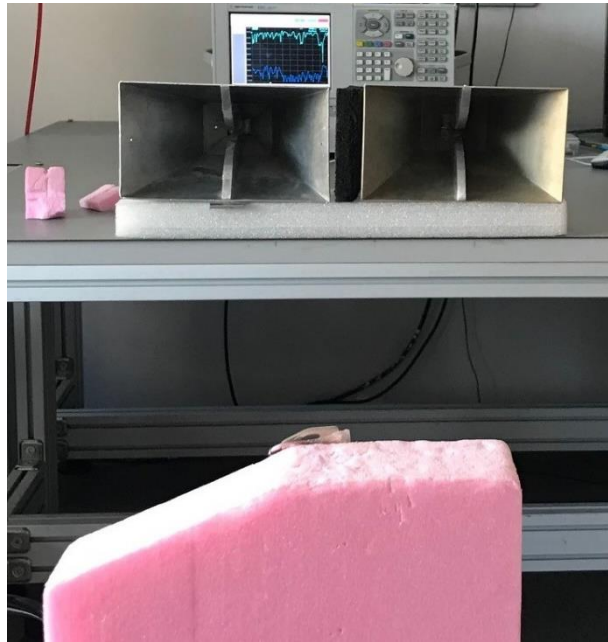
(a)
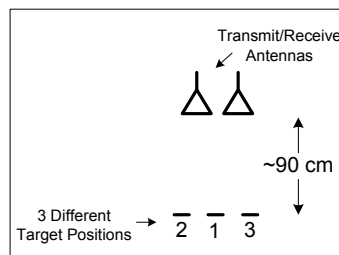
(b)

Figure 4. 2. MIMO Measurement Setup (a) Position#1 (b) Top View of the Setup with Target at Three Different Positions

Detection and False Alarm rates from the individual MIMO nodes, and the combined DRN case are given in the proceeding sections for MUSIC and Prony's Methods.

4.2.1. Application of the DRN MIMO to the Range Detection by MUSIC Method

Detection and False Alarm rates, P_d & P_{fa} for the individual MIMO nodes, and the combined DRN MIMO case, processed by MUSIC Method is given in Table 4. 3.

The enhancement by the implementation of the MIMO measurements can be seen from Table 4. 3. It can be realized from Table 4. 3.d. that the Pfa rates are reduced for the combined DRN case.

Table 4. 3. *P_d & P_{fa} Matrix with MUSIC Method (a) at Position#1, (b) at Position#2, (c) at Position#3, (d) after DRN MIMO application*

(a)

Targets	P_d	P_{fa}
PRF1	0.7	0.225
Sphere	0.9	0.2
GPS Ant.	0.6	0.35
Two Wire	0.6	0.3

(b)

Targets	P_d	P_{fa}
PRF1	0.7	0.025
Sphere	0.5	0.225
GPS Ant.	0.6	0.3
Two Wire	0.6	0.325

(c)

Targets	P_d	P_{fa}
PRF1	0.5	0.3
Sphere	0.7	0.225
GPS Ant.	0.9	0.15
Two Wire	1	0

(d)

Targets	P_d	P_{fa}
PRF1	0.7	0.1
Sphere	0.7	0.025
GPS Ant.	0.5	0.1
Two Wire	0.6	0.025

4.2.2. Application of the DRN MIMO to the Range Detection by Prony's Method

Pd & Pfa rates for the individual MIMO nodes, and the combined DRN MIMO case, processed by Prony's Method is given in Table 4. 4. It can be realized from Table 4. 4.d that the Pfa rates are reduced for the combined DRN case.

Table 4. 4. P_d & P_{fa} Matrix with Prony's Method (a) at Position#1, (b) at Position#1, (c) at Position#3, (d) after DRN MIMO application

(a)

Targets	P_d	P_{fa}
PRF1	0.7	0.5
Sphere	0.6	0.1
GPS Ant.	0.8	0.425
Two Wire	0.6	0.075

(b)

Targets	P_d	P_{fa}
PRF1	0.8	0.075
Sphere	0.6	0.525
GPS Ant.	0.7	0.5
Two Wire	0.7	0.25

(c)

Targets	P_d	P_{fa}
PRF1	0.5	0.175
Sphere	0.6	0.1
GPS Ant.	0.6	0.125
Two Wire	0.8	0

(d)

Targets	P_d	P_{fa}
PRF1	0.9	0.125
Sphere	0.6	0.1
GPS Ant.	0.9	0.275
Two Wire	0.8	0.025

4.2.3. Comparison and Enhancements

Comparing Table 4. 3.d and Table 4. 4.d, it can be stated that MUSIC method is better in terms of false alarm with less than 0.1 P_{fa} for all the candidate targets, and an average of 0.625 P_d. On the other hand; Prony's method shows an average detection 0.8 P_d, on the cost of P_{fa} as high as 0.275.

For the MIMO case, SNCR values are ~15 dB, ~11 dB, and ~11 dB for Position #1, 2, 3, respectively. Concerning the computation cost, MUSIC is more costly than Prony's. It might be concluded that increasing the SNCR value might increase the performance of the Prony's method to a comparable level with MUSIC method.

CHAPTER 5

CONCLUSIONS AND FUTURE WORK

This thesis focused on showing the proof of concept results for the detection of PRF1 in a practical, multi scatterer, echoic medium. Range detection performance for a set of resembling-spectrum objects, and detection & false alarm rates out of ten (10) measurements is presented. Prony's and MUSIC methods are compared and it is concluded that the performance of the MUSIC method is less prone to SNCR compared to Prony's method. In terms of modeling, MUSIC is more reliable since Prony's method models the poles of the system in a periodic manner.

The operational application of the method will result with a vast of data samples and the processing of these samples will be important in terms of giving the decision of detection or no detection. Intelligent processing is necessary in terms of determining the existence of PRF1 in the medium out of multiple detect/not detect decisions in time. It is expected that the vast of data samples will help increase the detection probability (P_d) if intelligently processed. A future work for examining the possible benefits of data processing on multiple time samples would be the realization of a multistatic scenario mimicking a dynamic environment with cooperative processing. This will give clues on the detection enhancement of cooperative data processing on multiple samples.

In terms of cooperative data processing, a statistical MIMO system with three (3) nodes is also implemented for utilizing the RCS diversity of the scatterers. Detection

in range is done by comparing the reference scatterer's complex spectrum by the range complex spectrum at incremental time (range) steps.

Adopted MUSIC method is the 1D MUSIC method usually used for the DoA. By the use of a coherent MIMO array, the steering vector; a in the MUSIC method can be reshaped to simultaneously detect the range and angle instead of sequentially applying the 1D MUSIC method in the two domains; range and angle [64]. This approach is called the 2D MUSIC method. The same approach can be used in our case with the proper steering vector formation for simultaneous range detection. The steering vector; a in this case will be 'node number' folded in terms of length. The cost of not scanning at incremental time steps will be working with a longer steering vector; hence with larger matrix and matrix operations. A profit-loss statement of the proposed method with the applied one should also be made.

REFERENCES

[1] M. Van Blaricum and R. Mittra, "A technique for extracting the poles and residues of a system directly from its transient response," in *IEEE Transactions on Antennas and Propagation*, vol. 23, no. 6, pp. 777-781, November 1975.

[2]C. E. Baum, E. J. Rothwell, K. M. Chen and D. P. Nyquist, "The singularity expansion method and its application to target identification," in *Proceedings of the IEEE*, vol. 79, no. 10, pp. 1481-1492, Oct 1991.

[3]S. Anuradha and J. Balakrishnan, "Discrimination of closely resembling PEC targets based on natural resonant frequencies," *2014 IEEE International Microwave and RF Conference (IMaRC)*, Bangalore, 2014, pp. 140-143.

[4]W. C. Chen and N. Shuley, "Utilizing the energy of each of the extracted poles to identify the dominant complex natural resonances of the radar target," *2007 IEEE Antennas and Propagation Society International Symposium*, Honolulu, HI, 2007, pp. 69-72.

[5]N. Gharsallah, E. J. Rothwell, K. M. Chen and D. P. Nyquist, "Identification of the natural resonance frequencies of a conducting sphere from a measured transient response," in *IEEE Transactions on Antennas and Propagation*, vol. 38, no. 1, pp. 141-143, Jan 1990.

[6]C. O. Hargrave, I. V. L. Clarkson and H. S. Lui, "Late-Time Estimation for Resonance-Based Radar Target Identification," in *IEEE Transactions on Antennas and Propagation*, vol. 62, no. 11, pp. 5865-5871, Nov. 2014.

[7] C. W. Chuang and D. L. Moffatt, "Natural resonances of radar targets via Prony's method and target discrimination," *IEEE Tmns. Aerospace Electron. Syst.*, vol. AES-12, no. 5, pp. 583-589, Sept.1976.

[8] N. H. Younan, C. M. Shearin and T. F. Nash, "Natural frequencies extraction of a radar target from a measured response using the Prony method," *The Record of the 1993 IEEE National Radar Conference*, Lynnfield, MA, USA, 1993, pp. 66-69.

[9] Chi-Chih Chen and L. Peters, "Buried unexploded ordnance identification via complex natural resonances," in *IEEE Transactions on Antennas and Propagation*, vol. 45, no. 11, pp. 1645-1654, Nov 1997.

[10] J. Makhoul, "Linear prediction: A tutorial review," in *Proceedings of the IEEE*, vol. 63, no. 4, pp. 561-580, April 1975.

[11] M. H. Hayes, Statistical Digital Signal Processing and Modeling, John Wiley & Sons Inc., New York, 1996.

[12] E. Rothwell, D. Nyquist, Kun-Mu Chen and B. Drachman, "Radar target discrimination using the extinction-pulse technique," in *IEEE Transactions on Antennas and Propagation*, vol. 33, no. 9, pp. 929-937, Sep 1985.

[13] E. Rothwell, Kun-Mu Chen, D. Nyquist and Weimin Sun, "Frequency domain E-pulse synthesis and target discrimination," in *IEEE Transactions on Antennas and Propagation*, vol. 35, no. 4, pp. 426-434, April 1987.

[14] E. Rothwell, Kun-Mu Chen and D. Nyquist, "Extraction of the natural frequencies of a radar target from a measured response using E-pulse techniques," in *IEEE Transactions on Antennas and Propagation*, vol. 35, no. 6, pp. 715-720, June 1987.

[15]   E. Kennaugh, "The K-pulse concept," in *IEEE Transactions on Antennas and Propagation*, vol. 29, no. 2, pp. 327-331, Mar 1981.

[16]   Turhan-Sayan, G, & Moffatt, D, "K-pulse estimation and target identification of low-Q radar targets", *Wave Motion*, vol. 11, no. 5, p. 453-461, 1989.

[17]   H. S. Lui, N. V. Z. Shuley and A. D. Rakic, "A Novel, Fast, Approximate Target Detection Technique for Metallic Target Below a Frequency Dependant Lossy Halfspace," in *IEEE Transactions on Antennas and Propagation*, vol. 58, no. 5, pp. 1699-1710, May 2010.

[18]   A. Gallego, A. Medouri and M. Carmen Carrion, "Estimation of number of natural resonances of transient signal using E-pulse technique," in *Electronics Letters*, vol. 27, no. 24, pp. 2253-2256, 21 Nov. 1991.

[19]   E. J. Rothwell and K. M. Chen, "A hybrid E-pulse/least squares technique for natural resonance extraction," in *Proceedings of the IEEE*, vol. 76, no. 3, pp. 296-298, Mar 1988.

[20]   P. Ilavarasan, J. E. Ross, E. J. Rothwell, K. M. Chen and D. P. Nyquist, "Performance of an automated radar target discrimination scheme using E pulses and S pulses," in *IEEE Transactions on Antennas and Propagation*, vol. 41, no. 5, pp. 582-588, May 1993.

[21]   Toribio, R, Saillard, J, & Pouliguen, P 2003, 'Identification of radar targets in resonance zone: E-Pulse techniques', *Progress in Electromagnetics Research*, vol. 43, p. 39-58.

[22] M. C. Carrion, A. Gallego, J. Porti and D. P. Ruiz, "Subsectional-polynomial E-pulse synthesis and application to radar target discrimination," in *IEEE Transactions on Antennas and Propagation*, vol. 41, no. 9, pp. 1204-1211, Sep 1993.

[23] H. Zhang, Z. Fan, D. Ding and R. Chen, "Radar Target Recognition Based on Multi-Directional E-Pulse Technique," in *IEEE Transactions on Antennas and Propagation*, vol. 61, no. 11, pp. 5838-5843, Nov. 2013.

[24] Q. Li, P. Ilavarasan, J. E. Ross, E. J. Rothwell, Kun-Mu Chen and D. P. Nyquist, "Radar target identification using a combined early-time/late-time E-pulse technique," in *IEEE Transactions on Antennas and Propagation*, vol. 46, no. 9, pp. 1272-1278, Sep 1998.

[25] Y. Hua and T. K. Sarkar, "A discussion of E-pulse method and Prony's method for radar target resonance retrieval from scattered field," in *IEEE Transactions on Antennas and Propagation*, vol. 37, no. 7, pp. 944-946, July 1989.

[26] J. D. Morales, D. Blanco, D. P. Ruiz and M. C. Carrion, "Non Cooperative Radar Target Identification Using Exponential Single-Mode Extraction Pulse," in *IEEE Transactions on Antennas and Propagation*, vol. 59, no. 6, pp. 2445-2447, June 2011.

[27] Y. Hua and T. K. Sarkar, "Generalized pencil-of-function method for extracting poles of an EM system from its transient response," in *IEEE Transactions on Antennas and Propagation*, vol. 37, no. 2, pp. 229-234, Feb. 1989.

[28] T. K. Sarkar, Sheeyun Park, Jinhwan Koh and S. M. Rao, "Application of the matrix pencil method for estimating the SEM (singularity expansion method) poles of source-free transient responses from multiple look directions," in *IEEE Transactions on Antennas and Propagation*, vol. 48, no. 4, pp. 612-618, Apr 2000.

[29] L. Man, X. Wei, C. Dong and Z. Xiao, "Poles Extracting and Analyzing of Complex Stealth Target Based on Matrix Pencil Method," *2014 IEEE International Conference on Computer and Information Technology*, Xi'an, 2014, pp. 894-898.

[30] Y. Hua and T. K. Sarkar, "Matrix pencil method for estimating parameters of exponentially damped/undamped sinusoids in noise," in *IEEE Transactions on Acoustics, Speech, and Signal Processing*, vol. 38, no. 5, pp. 814-824, May 1990.

[31] M. Khodjet-Kesba, K. El Khamlichi Drissi, S. Lee, C. Faure, C. Pasquier and K. Kerroum, "Robust UWB radar target classification in white Gaussian noise based on Matrix Pencil Method in Frequency Domain and Mahalanobis Distance," *2014 International Radar Conference*, Lille, 2014, pp. 1-5.

[32] R. Rezaiesarlak and M. Manteghi, "On the Application of Short-Time Matrix Pencil Method for Wideband Scattering From Resonant Structures," in *IEEE Transactions on Antennas and Propagation*, vol. 63, no. 1, pp. 328-335, Jan. 2015.

[33] W. Ketpan, S. Phonsri, R. Qian and M. Sellathurai, "On the Target Detection in OFDM Passive Radar Using MUSIC and Compressive Sensing," *2015 Sensor Signal Processing for Defence (SSPD)*, Edinburgh, 2015, pp. 1-5.

[34] F. Belfiori, W. van Rossum and P. Hoogeboom, "2D-MUSIC technique applied to a coherent FMCW MIMO radar," *IET International Conference on Radar Systems (Radar 2012)*, Glasgow, UK, 2012, pp. 1-6.

[35] Y. Zhang, G. Zhang and X. Wang, "Computationally efficient DOA estimation for monostatic MIMO radar based on covariance matrix reconstruction," in *Electronics Letters*, vol. 53, no. 2, pp. 111-113, 1 19 2017.

[36] Wei, W, Dong, L, Zhihua, W, Haiyang, Y, & Qi, L 2015, 'Design and Implementation of a FPGA and DSP Based MIMO Radar Imaging System', *Radioengineering, Vol 24, Iss 2, Pp 518-526 (2015)*, no. 2, p. 518.

[37] X. Zhang, L. Xu, L. Xu and D. Xu, "Direction of Departure (DOD) and Direction of Arrival (DOA) Estimation in MIMO Radar with Reduced-Dimension MUSIC," in *IEEE Communications Letters*, vol. 14, no. 12, pp. 1161-1163, December 2010.

[38] H. Meng, Z. Zheng, Y. Yang, K. Liu and Y. Ge, "A low-complexity 2-D DOA estimation algorithm for massive MIMO systems," *2016 IEEE/CIC International Conference on Communications in China (ICCC)*, Chengdu, 2016, pp. 1-5.

[39] J. F. Chen and H. Ma, "An accurate real-time algorithm for spectrum peaks search in 2D MUSIC," *2011 International Conference on Multimedia Technology*, Hangzhou, 2011, pp. 3385-3388.

[40] F. Belfiori, W. van Rossum and P. Hoogeboom, "Application of 2D MUSIC algorithm to range-azimuth FMCW radar data," *2012 9th European Radar Conference*, Amsterdam, 2012, pp. 242-245.

[41] J. Zhuang, J. Liu, D. Chen and N. Yu, "Low complexity 2-D DOA estimator for arbitrary arrays: A hybrid MUSIC-based method," *2015 10th International Conference on Information, Communications and Signal Processing (ICICS)*, Singapore, 2015, pp. 1-4.

[42] Y. Nechaev and I. Peshkov, "Impact of beamspace processing on accuracy of DOA estimation using MUSIC and Capon methods," *2015 38th International Conference on Telecommunications and Signal Processing (TSP)*, Prague, 2015, pp. 472-476.

[43] N. Sakar, G. Hislop and C. Craeye, "A post-processing approach to the MUSIC algorithm for 2D direction finding," *Proceedings of the 5th European Conference on Antennas and Propagation (EUCAP)*, Rome, 2011, pp. 3005-3008.

[44] M. Secmen and G. Turhan-Sayan, "A novel electromagnetic target recognition method by MUSIC algorithm," *2006 IEEE Antennas and Propagation Society International Symposium*, Albuquerque, NM, 2006, pp. 1299-1302.

[45] M. Secmen, G. Turhan-Sayan and A. Hizal, "Radar target recognition method with MUSIC algorithm: Application to aircraft targets with measured scattered data," *2008 IEEE Radar Conference*, Rome, 2008, pp. 1-6.

[46] M. Secmen, E. Ekmekci and G. Turhan-Sayan, "A resonance region method for recognition of multiple targets using the MUSIC algorithm and a time correlation technique," *2008 IEEE Antennas and Propagation Society International Symposium*, San Diego, CA, 2008, pp. 1-4.

[47] M. Secmen, "The application of fusion of multiple aspect scattered data to PMUSIC-vector based electromagnetic target identification," *2011 IEEE International Symposium on Antennas and Propagation (APSURSI)*, Spokane, WA, 2011, pp. 2750-2753.

[48] M. Secmen and G. Turhan-Sayan, "Radar target classification method with reduced aspect dependency and improved noise performance using multiple signal classification algorithm," in *IET Radar, Sonar & Navigation,* vol. 3, no. 6, pp. 583-595, December 2009.

[49] M. Secmen, "A Novel MUSIC Algorithm Based Electromagnetic Target Recognition Method In Resonance Region For The Classification Of Single And Multiple Targets," Ph.D. Dissertation, Middle East Technical University, 2008.

[50] J.A. Stratton, Electromagnetic Theory. New York: McGraw-Hill, 1941.

[51] J. L. Kerr, "Short axial length broad-band horns," *IEEE Trans. Antenna Propagat., AP-21*, 1973, pp. 710–714.

[52] "ETS-3117 datasheet", ETS-Lindgren Corporation, Cedar Park, USA.

[53] "R&S®HF907 datasheet", Rohde & Schwarz, Munich, Germany.

[54] "BBHA 9120 B", Schwarzbeck Mess - Elektronik OHG, Mannheim, Germany.

[55] C. A. Balanis, Advanced Engineering Electromagnetics, John Wiley & Sons Inc., New York, 1989.

[56] J. Van Bladel, Electromagnetic Fields, 2nd Ed., John Wiley & Sons Inc., New Jersey, 2007.

[57] L. R. Rabiner, R. W. Schafer, and C. M. Rader, "The chirp z-transform algorithm and its applications," Bell Sys. Tech. J., vol. 48, pp. 1249-1292, May 1969.

[58] Rabiner, Lawrence R., and Bernard Gold. *Theory and Application of Digital Signal Processing*. Englewood Cliffs, NJ: Prentice-Hall, 1975, pp. 393–399.

[59] Y. Li, J. Razavilar and K. J. Ray Liu, "DMUSIC algorithm for 2D NMR Signals," *Engineering in Medicine and Biology Society, IEEE 17th Annual Conference*, pp. 477 – 478, Sept. 1995.

[60] S. E. Fienberg, "An Iterative Procedure for Estimation in Contingency Tables," *Annals of Mathematical Statistics*, Vol. 41, No.3, pp. 907-917, June 1970.

[61] A.M. Haimovich, R.S. Blum and L.J. Cimini, "MIMO Radar with Widely Separated Antennas", *IEEE Signal Processing Magazine*, Vol. 25, Issue 1, pp. 116-129, 2008.

[62] J. Li, P. Stoica, *MIMO Radar Signal Processing*, John Wiley & Sons Inc., New Jersey, 2008.

[63] F. Belfiori, W. van Rossum and P. Hoogeboom, "Coherent MIMO Array Design With Periodical Physical Element Structures", *IEEE Antennas and Wireless Propagation Letters*, Vol. 10, pp. 1341-1344, 2011.

[64] F. Belfiori, W. van Rossum and P. Hoogeboom, "2D-MUSIC technique applied to a coherent FMCW MIMO radar," *IET International Conference on Radar Systems (Radar 2012)*, Glasgow, UK, 2012, pp. 1-6.

[65] F. Belfiori, G. Babur, P. Aubry and F. Le Chevalier, "Monopulse on transmit by means of orthogonal probing signals: Theoretical and experimental validations," *2014 International Radar Conference*, Lille, 2014, pp. 1-4.

[66] M. Skolnik, *Introduction to Radar Systems*, 3rd ed. New York: McGraw-Hill, 2001.

[67] E. Fishler, A. Haimovich, R. Blum, L. Cimini, D. Chizhik, and R. Valenzuela, "Spatial diversity in radars—Models and detection performance," IEEE Trans. Signal Processing, vol. 54, pp. 823–838, Mar. 2006.

TIME DOMAIN SCATTERING FROM A PERFECT CONDUCTING SPHERE

A.1. Scattering from a Conducting Sphere

Scattering from a conducting sphere is obtained theoretically from the solution of the wave equation expressed in terms of spherical wave functions [55]-[56]. The scattered fields in the far-field zone can be expressed as the sum of E_θ^{scat} and E_ϕ^{scat} scattered components since E_R^{scat} can be neglected in the far field. The scattered fields from a sphere in the far-field zone can be written in terms of spherical waves as follows:

$$E_\phi^{scat} = \frac{je^{-jk_0R}}{k_0R} sin\phi \sum_{n=1}^{\infty} \frac{2n+1}{n(n+1)} \left\{ a_n \frac{P_n^{(1)}(cos\theta)}{sin\theta} + b_n \frac{P_n^{(1)}(cos\theta)}{d\theta} \right\} \quad (A.1)$$

$$E_\theta^{scat} = \frac{je^{-jk_0R}}{k_0R} cos\phi \sum_{n=1}^{\infty} \frac{2n+1}{n(n+1)} \left\{ a_n \frac{P_n^{(1)}(cos\theta)}{d\theta} + b_n \frac{P_n^{(1)}(cos\theta)}{sin\theta} \right\} \quad (A.2)$$

where $P_n^{(1)}(cos\theta)$ are the associated first kind Legendre polynomials. a_n and b_n take the following forms for conducting spheres:

$$a_n = \frac{[d(xj_n(x))/dx]_{k_o a}}{\left[d(xh_n^{(2)}(x))/dx \right]_{k_o a}} \quad (A.3)$$

$$b_n = \frac{j_n(k_0a)}{h_n^{(2)}(k_0a)} \quad (A.4)$$

where $j_n(x)$ and $h_n^{(2)}(x)$ are spherical Bessel and Hankel functions. The above stated theoretical solution is used for obtaining the scattering form a conducting sphere subject to a linearly (+x) polarized incident wave, propagating in the +z direction as shown in *Figure A. 1*. The implementation is done in MATLAB ® for the scattered field of a 1.8 cm radius conducting sphere at $R = 72\ cm, \theta = 150°, \phi = 90°$. The frequency domain scattered fields E_ϕ^{scat} is zero, and E_θ^{scat} can be seen in *Figure A. 2*. The frequency range is 0-12 GHz, number of frequency samples is 874 with a resulting frequency resolution of 13.75 MHz.
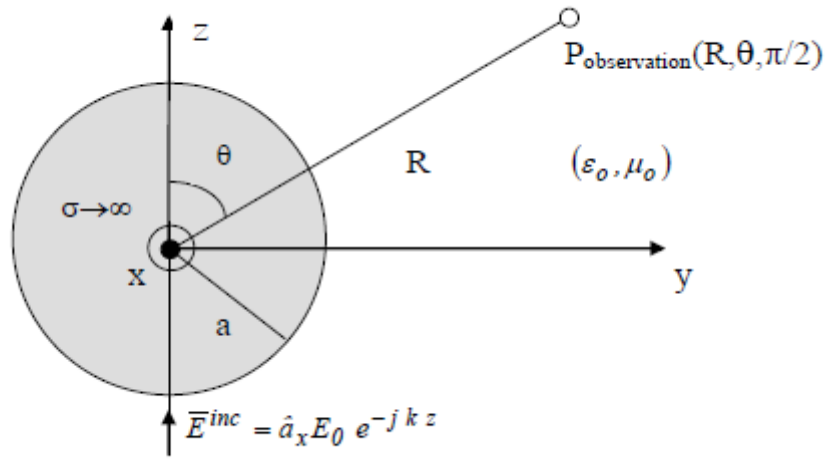

Figure A. 1. Conducting Sphere and the x-polarized z-propagating Incident Field
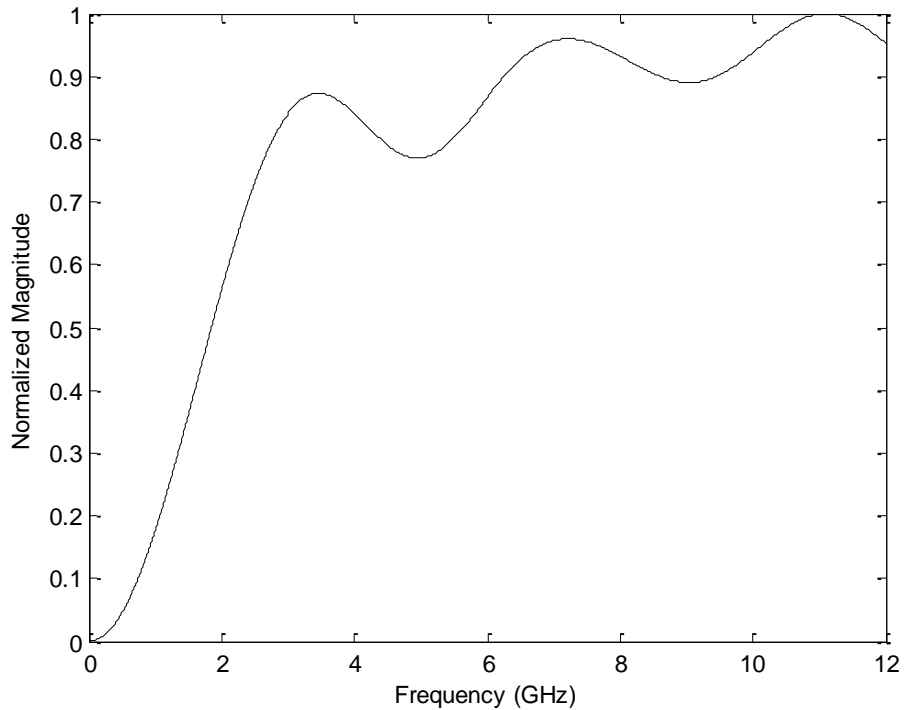
Figure A. 2. E_θ^{scat} from a 1.8 cm radius sphere at $R = 72\ cm, \theta = 150°, \phi = 90°$

A.2. Normal (Gaussian) Window

The time domain measurements in the Vector Network Analyzer (VNA) are the Inverse Chirp Z-Transform (ICZT) of the frequency domain measurements. The frequency domain measurements are multiplied by a window response due to finite frequency samples; a rectangular window if no other specific window is used. The rectangular window, however comes up with a Side Lobe Level (SLL) of -13 dB in time domain which may be accepted as high for many cases. This high SLL permits the undesired time domain responses to be involved in the measurements. The modified windows are used which are with lower SLLs but with wider bandwidths in return. The most widely used window is the Normal (Gaussian) Window which has -44 dB SLL in the time domain response. The Normal Window in frequency domain, and the corresponding Inverse Fast Fourier Transform can be seen in *Figure A. 3.*
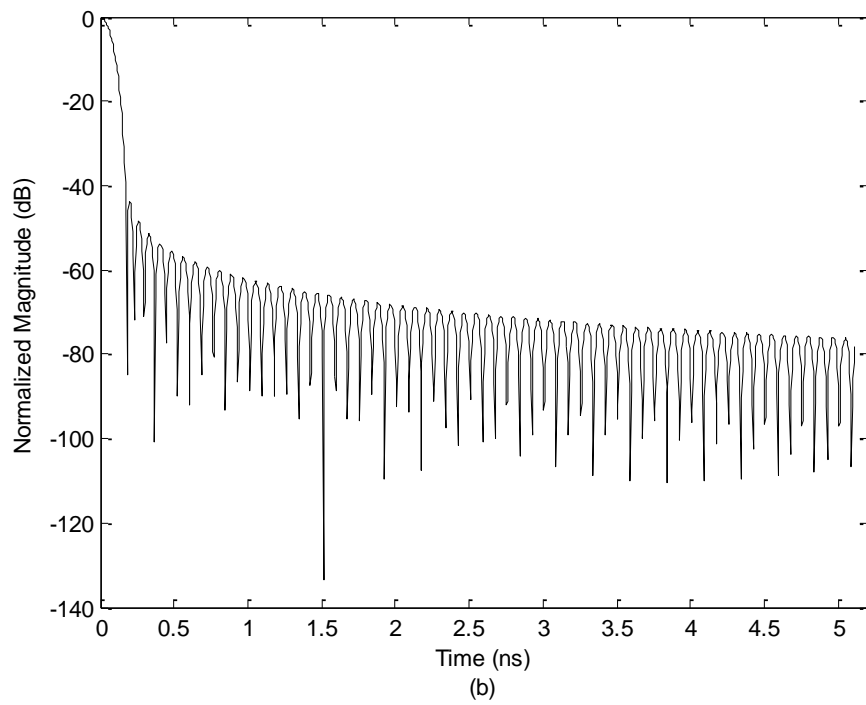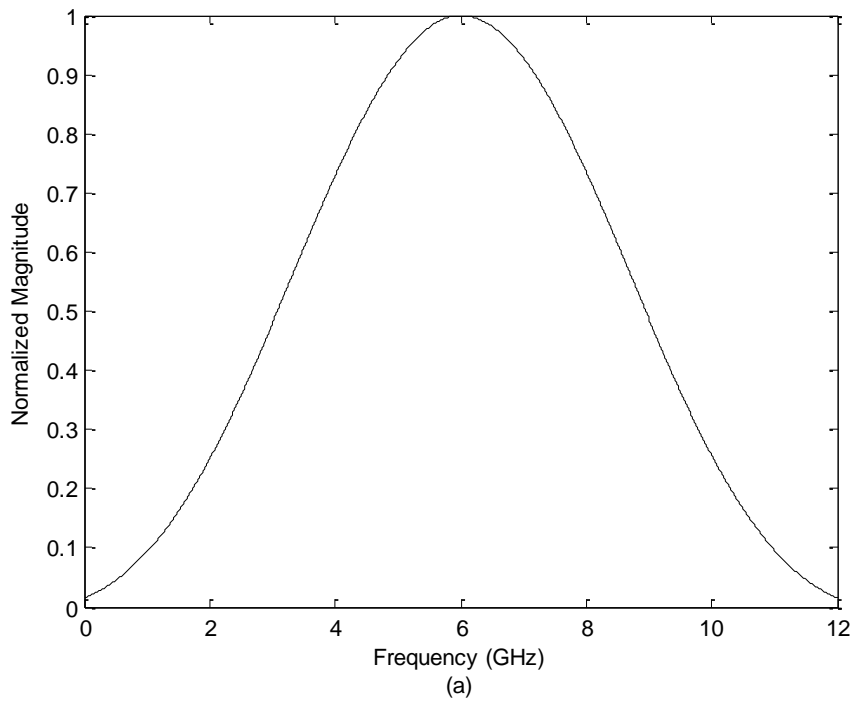
Figure A. 3. Normal Window (a) Frequency Domain (b) Time Domain Response

A.3. Inverse Chirp Z-Transform (ICZT)

Chirp Z-Transform (CZT) is a computational algorithm developed to evaluate the M-point Z-Transform of a sequence of N-samples [57]-[58]. Z-Transform for a sequence of finite numbers N of non-zero points is:

$$X_k = X(z_k) = \sum_{n=0}^{N-1} x_n z_k^{-n} \quad k = 0, \dots, N-1. \tag{A.5}$$

where sum converges except $z = 0$ and X_k can be computed at a finite number of points z_k. The special set of z_k :

$$z_k = e^{j2\pi k \backslash N} \quad k = 0, \dots, N-1. \tag{A.6}$$

corresponds to the well-known DFT:

$$X_k = \sum_{n=0}^{N-1} x_n e^{-j\frac{2\pi k}{N}n} \quad k = 0, \dots, N-1. \tag{A.7}$$

It is easily noticed that the values of z_k are the Nth roots of unity which means that the sampling is done at the full '2π' contour at N equally spaced angles on the unity gain complex frequency $'\omega'$ circle of *Figure A. 4*.

CZT is a more generalized form of the DFT with M sample points in the Z-domain:

$$C_k = C(z_k) = \sum_{n=0}^{N-1} x_n z_k^{-n} \quad ; \qquad z_k = AW^{-k} \quad k = 0, \dots, M-1. \tag{A.8}$$

where A & W are arbitrary complex numbers. Depending on the selection of A and W; the sampling contour can be chosen.
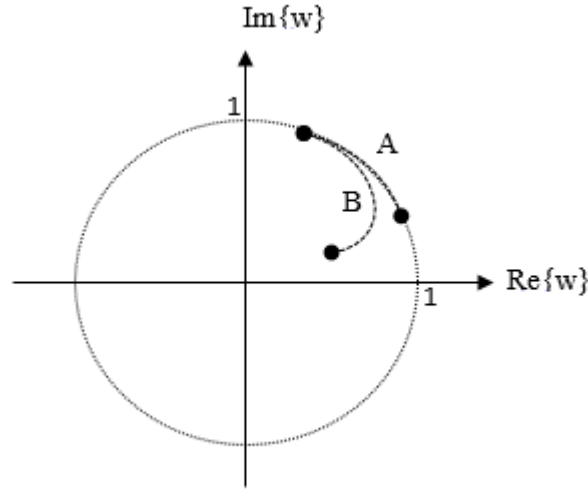
Figure A. 4. Complex Frequency Domain Representation for IDFT and ICZT

Starting with a pre-defined set of frequencies; the Inverse DFT (IDFT) results with the time series bounded by the resolution and sample point of the initial data:

$$t_{resoln} = \frac{1}{(f_{max} - f_{min}) \times N} \tag{A.9}$$

where f_{min}, f_{max}, and N are the start, end frequencies and the number of points of the frequency domain sequence respectively. t_{resoln} is the resulting resolution of the time domain sequence.

Considering the Vector Network Analyzer (VNA) measurements as an instant case, the bound brought by IDFT is not acceptable. There is a need for the flexible selection of the start and end times of the sequence to be evaluated. Additionally, flexibility in terms of resolution is also necessary. The application of the Inverse CZT (ICZT) is launched at this point. Instead of the full 2π contour of *Figure A. 4*, contour 'A' is chosen:

$$x_n = c(Z_n) = \frac{1}{M} \sum_{k=0}^{M-1} C_k Z_n^k \quad ; \qquad Z_n = AW^n \quad n = 0, \dots, N-1. \tag{A.10}$$

72

where $A = -j2\pi \dfrac{\frac{t_{start}}{M}}{(f_{max}-f_{min})}$ and $W = j\dfrac{2\pi}{N}\dfrac{\frac{(t_{end}-t_{start})}{M}}{(f_{max}-f_{min})}$

With the proper selection of $Z_n = AW^{-n}$ (A.10), the desired time interval $(t_{end} - t_{start})$ can be zoomed with full usage of number of points. It is advisable not to forget that, still the time resolution, t_{resoln} is restricted by the start, end frequencies (A.9).

With the above mentioned properties of the ICZT, the time domain scattered field can be obtained in the desired resolution. *Figure A. 5* shows the windowed time domain response of the conducting sphere in a large scale, and a zoomed version.
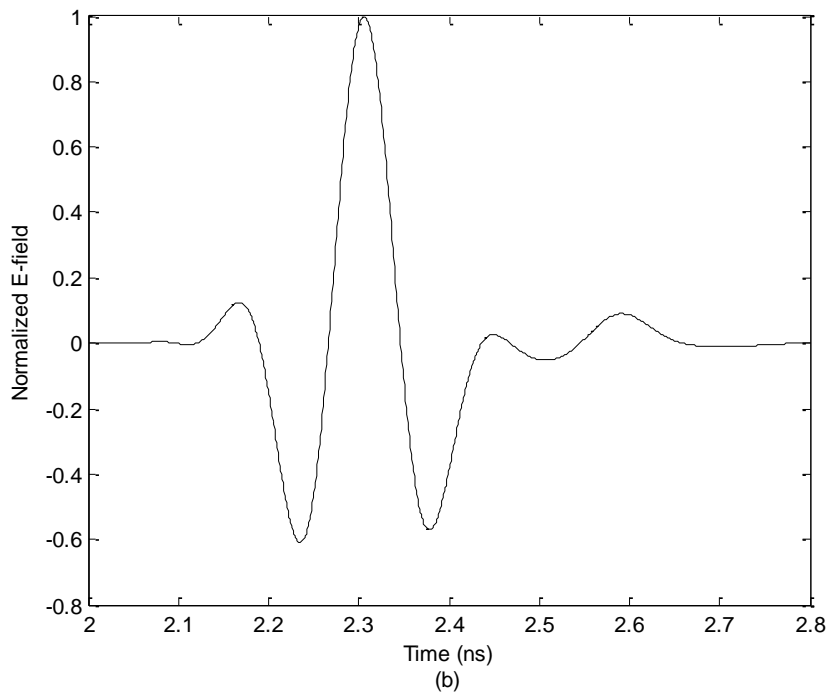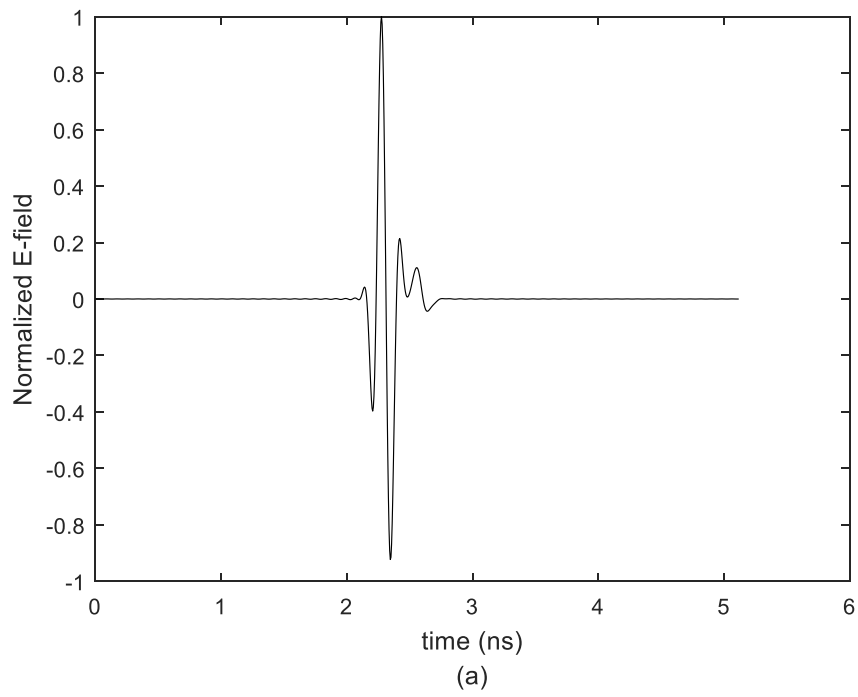
(a)

(b)

Figure A. 5. E_θ^{scat} from a 1.8 cm radius sphere; Windowed Time Domain Response (a) Time Scale 0-5.115 ns (b) Time Scale 2-2.8 ns

APPENDIX B

MATLAB CODES FOR ICZT OF A PERFECT CONDUCTING SPHERE

```matlab
function [esTheta, esPhi] = mieScatteredField(An, Bn, theta, phi, frequency)
% Rr=0.72;  % 72 cm ötedeki bir küre için yazdık !!!!!!!!!!!!!!!!!!!!!!!!!!!!
% Compute the complex-value scattered electric far field of a sphere
% using pre-computed coefficients An and Bn. Based on the treatment in:
% Ruck, et. al. "Radar Cross Section Handbook", Plenum Press, 1970.
% The incident electric field is in the -z direction (theta = 0) and is
% theta-polarized. The time-harmonic convention exp(jwt) is assumed, and
% the Green's function is of the form exp(-jkr)/r.
%
% Inputs:
%   An: Array of Mie solution constants
%   Bn: Array of Mie solution constants
%      (An and Bn should have the same length)
%   theta: Scattered field theta angle (radians)
%   phi: Scattered field phi angle (radians)
% Outputs:
%   esTheta: Theta-polarized electric field at the given scattering angles
%   esPhi: Phi-polarized electric field at the given scattering angles
%
%   Output electric field values are normalized such that the square of the
%   magnitude is the radar cross section (RCS) in square meters.
%
%   Author: Walton C. Gibson, email: kalla@tripoint.org
% Reorganized by Ozgehan Kilic
 Rr=0.72;  % 72 cm ötedeki bir küre için yazdık
% speed of light
c = 299792458.0;
 % wavenumber
k = 2.0*pi*frequency/c;

sinTheta = abs(sin(theta)); % note: theta only defined from from 0 to pi
cosTheta = cos(theta); % ok for theta > pi
```

```matlab
 % first two values of the Associated Legendre Polynomial
plm(1)  = -sinTheta;
plm(2)  = -3.0*sinTheta*cosTheta;
S1 = 0.0;
S2 = 0.0;
p = plm(1);
% compute coefficients for scattered electric far field
for iMode = 1:length(An)
      % derivative of associated Legendre Polynomial
    if abs(cosTheta) < 0.999999
       if iMode == 1
          dp = cosTheta*plm(1)/sqrt(1.0  - cosTheta*cosTheta);
       else
          dp = (iMode*cosTheta*plm(iMode) - (iMode + 1)*plm(iMode - 1))/sqrt(1.0 - cosTheta*cosTheta);
       end
    end
       if abs(sinTheta) > 1.0e-6
       term1  = An(iMode)*p/sinTheta;
       term2  = Bn(iMode)*p/sinTheta;
    end
    coeffi=(2*iMode+1)/(iMode*(iMode+1));
    uss=(-1)^iMode;
    if cosTheta > 0.999999
       % Ruck, et. al. (3.1-12)
       %val = ((i)^(iMode-1))*(iMode*(iMode+1)/2)*(An(iMode)  - i*Bn(iMode));
       val = ((2*iMode+1)/2)*(An(iMode)  + Bn(iMode));
       S1 = S1 + val;
       S2 = S2 + val;
    elseif cosTheta < -0.999999
       % Ruck, et. al. (3.1-14)
       %val = ((-i)^(iMode-1))*(iMode*(iMode+1)/2)*(An(iMode)  + i*Bn(iMode));
       val = (uss*(2*iMode+1)/2)*(An(iMode) + Bn(iMode));
       S1 = S1 + val;
       S2 = S2 + val;
    else
       % Ruck, et. al. (3.1-6)
       %S1 = S1 + ((i)^(iMode+1))*(term1  - i*Bn(iMode)*dp);
       S1 = S1 + coeffi*(term1+Bn(iMode)*dp);
       % Ruck, et. al. (3.1-7)
       %S2 = S2 + ((i)^(iMode+1))*(An(iMode)*dp  - i*term2);
       S2 = S2 + coeffi*(An(iMode)*dp +term2);
    end
       % recurrence relationship for next Associated Legendre Polynomial
       if iMode > 1
       plm(iMode + 1) = (2.0*iMode + 1)*cosTheta*plm(iMode)/iMode - (iMode + 1)*plm(iMode - 1)/iMode;
    end
```

```
    p = plm(iMode + 1);
end
% complex-value scattered electric far field, Ruck, et. al. (3.1-5)
esTheta = S1*cos(phi);
esPhi = -S2*sin(phi);
 % normalize electric field so square of magnitude is RCS in square meters
%esTheta = esTheta*sqrt(4.0*pi)/k;
%esPhi = esPhi*sqrt(4.0*pi)/k;
Ur=1i*exp(-1i*k* Rr)/(k*Rr);
esTheta = esTheta*Ur;
esPhi = esPhi*Ur;
return
function [esTheta, esPhi] = mie(radius, frequency, theta, phi, nMax)
% Rr=0.72; % 72 cm ötedeki bir küre için yazdık !!!!!!!!!!!!!!!!!!!!!!
% Compute the complex-value scattered electric far field of a perfectly
% conducting sphere using the mie series. Follows the treatment in
% Chapter 3 of

% Ruck, et. al. "Radar Cross Section Handbook", Plenum Press, 1970.
%
% The incident electric field is in the -z direction (theta = 0) and is
% theta-polarized. The time-harmonic convention exp(jwt) is assumed, and
% the Green's function is of the form exp(-jkr)/r.
%
% Inputs:
%   radius: Radius of the sphere (meters)
%   frequency: Operating frequency (Hz)
%   theta: Scattered field theta angle (radians)
%   phi: Scattered field phi angle (radians)
%   nMax: Maximum mode for computing Bessel functions
% Outputs:
%   esTheta: Theta-polarized electric field at the given scattering angles
%   esPhi: Phi-polarized electric field at the given scattering angles
%
%   Output electric field values are normalized such that the square of the
%   magnitude is the radar cross section (RCS) in square meters.
%
%   Author: Walton C. Gibson, email: kalla@tripoint.org
 % speed of light
c = 299792458.0;
 % radian frequency
w = 2.0*pi*frequency;
 % wavenumber
k = w/c;
 % conversion factor between cartesian and spherical Bessel/Hankel function
s = sqrt(0.5*pi/(k*radius));
```

77

```
 % mode numbers
mode = 1:nMax;
 % compute spherical bessel, hankel functions
[J(mode)]  = besselj(mode + 1/2, k*radius); J = J*s;
[H(mode)]  = besselh(mode + 1/2, 2, k*radius); H = H*s;
[J2(mode)]  = besselj(mode + 1/2 - 1, k*radius); J2 = J2*s;
[H2(mode)]  = besselh(mode + 1/2 - 1, 2, k*radius); H2 = H2*s;
% derivatives of spherical bessel and hankel functions
% Recurrence relationship, Abramowitz and Stegun Page 361
% ben burada Page 439 daki formulu aldım !!!!!!!!!!!!!!!!!!!!!!!!!!!
%kaJ1P(mode)  = (k*radius*J2 - mode .* J );
%kaH1P(mode)  = (k*radius*H2 - mode .* H );
kaJ1P(mode)  = (k*radius*J2 - (mode+1) .* J );
kaH1P(mode)  = (k*radius*H2 - (mode+1) .* H );
 % Ruck, et. al. (3.2-1)
%An = -((i).^mode) .* ( J ./ H ) .* (2*mode + 1) ./ (mode.*(mode + 1));
% Ruck, et. al. (3.2-2), using derivatives of bessel functions
%Bn = ((i).^(mode+1)) .* (kaJ1P ./ kaH1P) .* (2*mode + 1) ./ (mode.*(mode + 1));
 %MSecmen tez Appendix, An ve Bn'in isimlerini değistirdim
Bn = kaJ1P ./ kaH1P;
An = J ./ H ;
[esTheta esPhi] = mieScatteredField(An, Bn, theta, phi, frequency);
return
```

CURRICULUM VITAE

PERSONAL INFORMATION

Surname, Name: Kılıç, Özgehan
Nationality: Turkish (TC)
Date and Place of Birth: 9 November 1985, Adana
email: ozgehansahin@gmail.com

EDUCATION

Degree	Institution	Year of Graduation
MS	METU Electrical and Electronics Engineering	2010
BS	METU Electrical and Electronics Engineering	2008
High School	Adana Ticaret Odası Anadolu Lisesi, Adana	2003

WORK EXPERIENCE

Year	Place	Enrollment
2018-Present	ROKETSAN Missiles Inc.	Senior RF Systems Engineer
2014-2018	HAVELSAN EHSIM	RF Design Engineer
01-09 2013	ETA Elektronik	Consultant
2012-2013	The Scientific and Technological Research Council of Turkey	Researcher
01-12 2011	Parlar Foundation	Consultant
2008-2010	The Scientific and Technological Research Council of Turkey	Researcher
2008-2014	METU Electrical and Electronics Engineering	Research and Teaching Assistant

FOREIGN LANGUAGES

Advanced English, Intermediate German

PUBLICATIONS

1. O. Kilic, I. Comart, S. Demir, and T. Akin, "3-bit CPW Phase Shifter Implemented by a Reduced Branch Line Coupler," The 13th International. Symposium on RF MEMS and RF Microsystems (MEMSWAVE 2012), Antalya, Turkey, 2-4 July 2012.

2. O. Kilic, A. Yalim, C. Cetintepe and S. Demir, "Calibration quality analysis of phased array antennas," Proceedings of the 2012 IEEE International Symposium on Antennas and Propagation, Chicago, IL, 2012, pp. 1-2.

3. O. Kilic and S. Demir, "Design of a two layer aperture-coupled unequal power divider," 2010 10th Mediterranean Microwave Symposium, Guzelyurt, 2010, pp. 33-35.

4. O. Kilic and S. Demir, "Design of a defected ground beam forming network," 2010 10th Mediterranean Microwave Symposium, Guzelyurt, 2010, pp. 307-309.

HOBBIES

Yoga, Lego